tion was terminated by adding 8.8 μl of the gel loading solution and a further incubation at 95 °C for 3 min. The reaction of REV1 was performed in the same manner as the reaction of pol κ with the exception that the standard reaction time was 5 min. For pol η, a ×10 reaction buffer containing 400 mM Tris-HCl (pH 8.0), 10 mM $MgCl_2$, 100 mM DTT, 1 mg/ml bovine serum albumin, and 450 mM KCl was used instead of the ×10 TLS buffer. The ^{32}P-labeled fragments were denatured and electrophoresed in a 9.5% polyacrylamide gel containing 8 M urea. The radioactivity of the fragments was determined using a Bio-Imaging Analyzer (BAS2500, Fuji Photo Film, Kanagawa, Japan). Kinetic parameters were determined by steady-state gel kinetic assays under similar conditions as described above. The incubation time for pol κ was changed to 10 min. K_m and k_{cat} were evaluated from the plot of the initial velocity *versus* the dCTP or dGTP concentration using a hyperbolic curve-fitting program in SigmaPlot 11 (Systat Software, Inc.). Data from two or three independent experiments were plotted together.

RESULTS

Construction of Template Oligonucleotides Containing a PhIP Adduct—We designed oligonucleotides containing a dG-C8-PhIP adduct at specific sites for use as templates in *in vitro* DNA synthesis analyses. For this purpose, we selected the 5′-TCCGGGAAC-3′ sequence as: 1) it corresponds to codon 868–870 of the rat *Apc* gene, one of three mutation hot spots (a single base deletion of G) in PhIP-induced colon tumors (21), and could thus be used as a model template that would reconstitute mutations of this gene; 2) two other mutation hot spots in the rat *Apc* gene and many mutated sites induced by PhIP in cultured cells and animal models contain 5′-GGGA-3′ as a core sequence (17–20). We thus speculated that the 5′-TCCGGGAAC-3′ sequence could be used as a model sequence for these GGGA to GGA mutations to some extent; and 3) some mutagenic compounds forming dG adducts, including PhIP, are expected to react preferentially with the 5′-G of a GG dinucleotide site when compared with a single G residue (31). We thus selected a sequence containing GGG as a template for our initial analysis.

We have recently synthesized three 9-mer oligonucleotides separately harboring a PhIP adduct on each G within the sequence 5′-TCC GGG AAC-3′ (22). Three 32-mer template oligonucleotides, p32B, p32C, and p32D, were constructed in our present study by ligation of these 9-mer oligonucleotides containing the dG-PhIP adduct with a 23-mer oligonucleotide, p23a, (Table 1 and supplemental Fig. S1). The purities of these oligonucleotides were tested after resolution by electrophoresis. In our present study, we principally describe the results of our *in vitro* DNA synthesis analysis using p32C as the template to avoid complexity.

In Vitro DNA Synthesis by A- and B-family DNA Polymerase—Many of the chemical compounds that can form DNA adducts *in vivo* and that show mutagenicity have been reported to impede the progress of DNA synthesis to different extents. The molecular size of PhIP is greater than most other mutagenic chemicals that form adducts. Hence, dG-PhIP was expected to block DNA synthesis to a considerable extent. To examine the effects of the dG-C8-PhIP adduct upon DNA synthesis, primer

TABLE 1
Oligonucleotide templates and primers

Oligonucleotide	Sequence[a]
p32A	5′-TCC GGG AAC TGACTCGTC GTGACTGGG AAAAC-3′
p32B	5′-TCC **G**GG AAC TGACTCGTC GTGACTGGG AAAAC-3′
p32C	5′-TCC G**G**G AAC TGACTCGTC GTGACTGGG AAAAC-3′
p32D	5′-TCC GG**G** AAC TGACTCGTC GTGACTGGG AAAAC-3′
p29	5′-GTT TTC CCA GTCACGACG AGTCAGTTC CC-3′
p28	5′-GTT TTC CCA GTCACGACG AGTCAGTTC C-3′
p27	5′-GTT TTC CCA GTCACGACG AGTCAGTTC-3′
p26	5′-GTT TTC CCA GTCACGACG AGTCAGTT-3′
p22	5′-GTT TTC CCA GTCACGACG AGTC-3′
p17	5′-GTT TTC CCA GTCACGAC-3′

[a] The bold G indicates the site of the PhIP-C8-dG adduct. Underlined sequences correspond to codon 868–870 at nucleotides 2602–2610 of the rat APC gene.

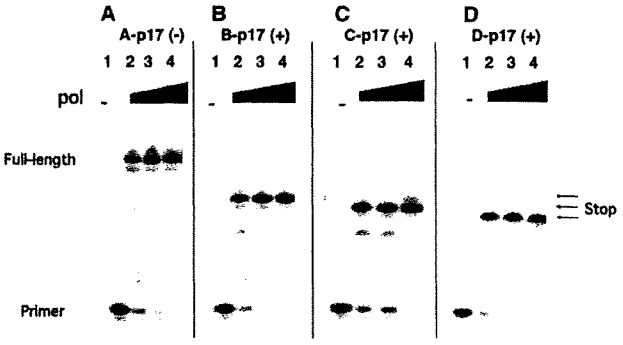

FIGURE 2. ***In vitro* DNA synthesis using Klenow fragment.** Gel electrophoresis indicating the primer extensions obtained using the 32-mer oligonucleotide templates, p32A (*A*), p32B (*B*), p32C (*C*), and p32D (*D*), which have no PhIP adduct, and a PhIP adduct on the first, second, and third G within the triple G sequence, respectively. The 3′ complementary 17-mer sequence, p17, was used as the extension primer. The final concentration of each template-primer complex was 12.5 nM. Concentrations of Klenow fragment were 0 (*lane 1*), 7.8 (*lane 2*), 23 (*lane 3*), and 78 units/ml (*lane 4*).

extension experiments using p32B, p32C, and p32D as templates were carried out (see Table 1). The length of each produced fragment was precisely determined using ladders of oligonucleotide fragments as markers (data not shown). The Klenow fragment of *E. coli* DNA polymerase I, a member of the A-family DNA polymerases, was first used in this analysis. The production of a 28-, 27-, and 26-mer from these primer extension reactions using B-p17, C-p17, and D-p17, respectively, using a template-primer complex, and lack of longer fragments indicated that the Klenow fragment stalled just before the dG-C8-PhIP adduct (Fig. 2). On the other hand, control experiments using p32A without the adduct as a template produced a 32-mer fragment (Fig. 2*A*). Similar results were obtained with *E. coli* DNA polymerase I (exo$^+$) and B-family DNA polymerases, such as the thermophilic bacterial DNA polymerases, r*Taq* and *Tth*, and human DNA polymerase α (data not shown) (supplemental Fig. S2), suggesting that stalling at the dG-C8-PhIP adduct occurs for all replicative DNA polymerases. Stalling of r*Taq* and *Tth* at the PhIP adduct was observed at 65 °C, as well as at 37 °C, indicating that this is the result of a physical hindrance of the adduct itself and not from secondary DNA structures. Moreover, there was no difference found between the stalling of *E. coli* DNA polymerase I (exo$^+$) and that of the Klenow fragment (exo$^-$). This indicates that the physical blocking of DNA polymerases at the dG-C8-PhIP adduct does not depend upon their proofreading function.

Finally, DNA synthesis analyses with human DNA polymerase δ (pol δ), a member of the B-family DNA polymerases and a truly replicative polymerase, were carried out. In the case of using p32C and p17 (C-p17) as a template-primer complex, the production of 27-mer fragments indicated the stalling of pol δ just before the PhIP adduct (Fig. 3, *lane 11*). From a control reaction using A-p17, a template-primer complex without the PhIP adduct, a full-length product of 32-mer was generated (Fig. 3, *lane 8*). In addition to these major products, minor products extended one nucleotide further (28- and 33-mer) and ladders of bands indicating degradation of primer (<17-mer) were observed (Fig. 3), corresponding with previous results reporting terminal dA transferase and exonuclease activities of pol δ (32). PCNA, an accessory protein acting as a sliding clamp for pol δ, was previously reported to promote DNA synthesis by pol δ past several template lesions, including abasic sites, 8-oxo-dG, and aminofluorene-dG (32). In the case of dG-C8-PhIP, however, PCNA was unable to promote the bypass synthesis of pol δ beyond the lesion (Fig. 3, *lane 12*). Extension reaction from the longer 22-mer primer, p22, also paused completely just before the PhIP adduct in the presence or absence of PCNA (Fig. 3, *lanes 5* and *6*). These results strongly suggest that the dG-C8-PhIP adduct on genome DNA in the living cells induces the complete block of replication forks including pol δ, PCNA, and pol α.

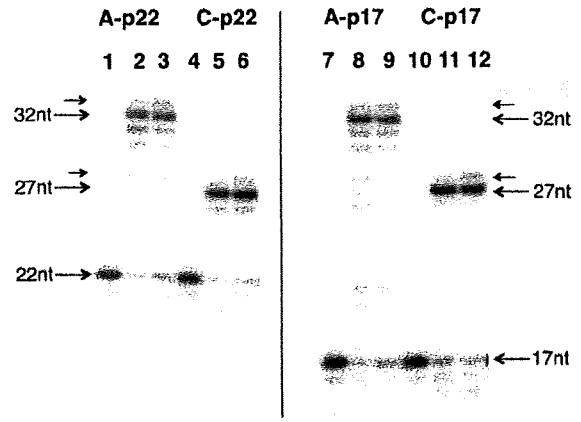

FIGURE 3. ***In vitro* DNA synthesis using pol δ in the presence or absence of PCNA.** Gel electrophoresis indicating the primer extensions obtained using the 32-mer oligonucleotide templates, p32A (*A*), and p32C (C), which have no PhIP adduct, and a PhIP adduct on the second G within the triple G sequence, respectively. The 3′ complementary 22- and 17-mer sequences, p22 and p17, were used as the extension primer. The final concentration of each template-primer complex was 12.5 nM. Concentrations of pol δ were 0 (*lanes 1, 4, 7,* and *10*) and 16 nM (*lanes 2, 3, 5, 6, 8, 9, 11,* and *12*). Concentrations of PCNA as a trimer were 0 (*lanes 1, 2, 4, 5, 7, 8, 10,* and *11*) and 20 nM (*lanes 3, 6, 9,* and *12*). *Large arrows* indicate the positions of primers (17- or 22-mer), full-length products (32-mer), and the products pausing just before the PhIP adduct (27-mer). *Small arrows* indicate the minor products that incorporated an additional 1 nucleotide (*nt*) to a full-length product or the pausing product.

Translesional DNA Synthesis by Y-family DNA Polymerases—Translesional DNA synthesis at the dG-C8-PhIP adduct by the Y-family DNA polymerases, pol η, pol κ, pol ι, and REV1 was next examined. Two substrates, C-p27 and C-p28, and their counterparts without a PhIP adduct, A-p27 and A-p28, were used in these experiments (Fig. 4). Substrate C-p27 was prepared by annealing the p32C template (see Table 1) to its 3′-complimentary 27-mer sequence, p27, and was used to identify the nucleotides that are inserted opposite the dG-C8-PhIP adduct (Fig. 4). Similarly, substrate C-p28 was used to analyze the extension reaction from the 3′-end of the dC bases opposite the dG-C8-PhIP adduct (Fig. 4). We found that recombinant human DNA polymerase η (pol η) could insert a dC opposite the dG-C8-PhIP adduct, although at low efficiency compared with control experiments without the PhIP adduct (Fig. 5, *A* and *B*). Extension reactions catalyzed by pol η from the 3′-end of dC opposite the adduct were barely detectable (Fig. 5*D*), although an excessive amount of pol η produced byproducts that incorporated a mismatch nucleotide, dG, dA, or dT (supplemental Fig. S4). In the case of dG, incorporation of one to three dG nucleotides was observed (supplemental Fig. S4). In control experiments without the PhIP adduct, minor products were produced that incorporated mismatch nucleotides, in addition to a major product that incorporated a dC (Fig. 5*C*).

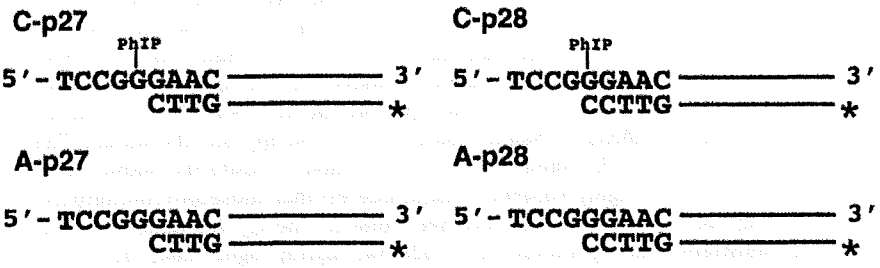

FIGURE 4. **Template-primer complexes.** Substrates C-p27 and C-p28 (series-C) have a PhIP adduct on the second dG within a GGG sequence. Substrates A-p27 and A-p28 (series-A) are control substrates without a PhIP adduct. The corresponding 3′ complimentary 27- and 28-mer sequences, p27 and p28, were used as extension primers. The template-primer complexes, C-p27 and C-p28, were used to monitor the nucleotide insertions into the site opposite dG-C8-PhIP and the extension reactions from the 3′-dC opposite dG-C8-PhIP, respectively.

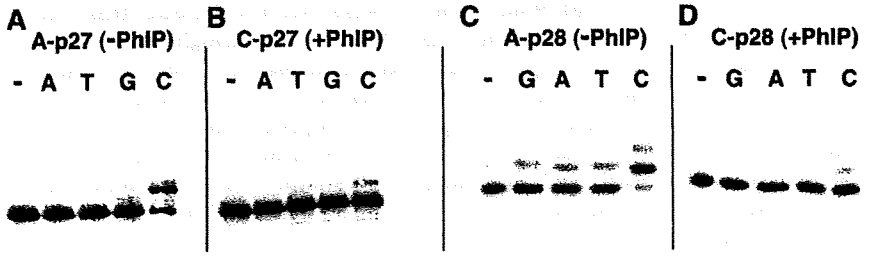

FIGURE 5. **Translesional DNA synthesis by pol η using substrates C-p27 and C-p28.** Control reactions were performed using substrates without the PhIP adduct, A-p27 (*A*) and A-p28 (C). An insertion reaction was performed with substrate C-p27 (*B*) and an extension reaction with substrate C-p28 (*D*). A single dNTP (G, A, T, C) was added into the reaction mixture as indicated by *G, A, T,* and *C above* each lane. The lanes indicated by − are controls without any nucleotides. Concentrations of pol η and each dNTP were 1.9 nM and 100 μM, respectively.

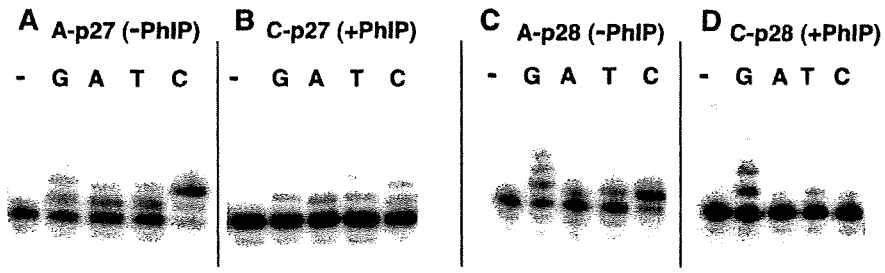

FIGURE 6. **Translesional DNA synthesis by pol κ using substrates C-p27 and C-p28.** Control reactions were performed using substrates without the PhIP adduct, A-p27 (*A*) and A-p28 (*C*). An insertion reaction was performed with substrate C-p27 (*B*) and an extension reaction with substrate C-p28 (*D*). A single dNTP (G, A, T, C) was added into the reaction mixture as indicated by *G*, *A*, *T*, and *C above* each lane. The lanes indicated by − are controls without any nucleotides. The concentrations of pol κ were 250 (*A* and *C*), 500 (*B*), and 1000 nM (*D*), respectively. The concentration of each dNTP was 100 μM.

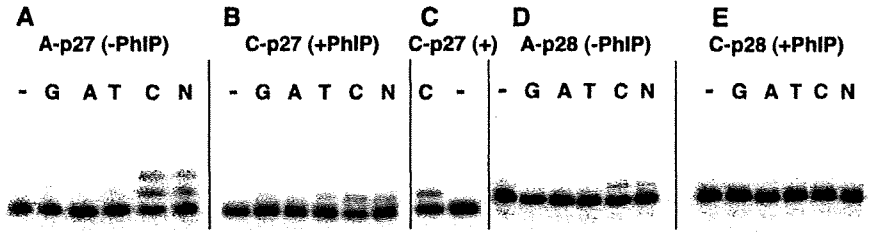

FIGURE 7. **Translesional DNA synthesis by REV1 using substrates C-p27 and C-p28.** Control reactions were performed using substrates without the PhIP adduct, A-p27 (*A*) and A-p28 (*D*). Insertion reactions were performed with substrate C-p27 (*B* and *C*) and an extension reaction with substrate C-p28 (*E*). A single dNTP (G, A, T, and C) or a mixture of each was added into the reaction mixture as indicated by *G*, *A*, *T*, *C*, and *N above* each lane. The lanes indicated by − are controls without any nucleotides. The concentrations of REV1 were 5.2 (*A* and *D*) and 26 nM (*B*, *C*, and *E*), respectively. The concentrations of each dNTP were 100 μM (*A*, *B*, *D*, and *E*) and 320 μM (*C*), respectively. The *N* mixture contained each dNTP at a concentration of 25 μM.

We next examined translesional DNA synthesis beyond the PhIP adduct using a truncated form of human DNA polymerase κ containing the N-terminal 559 amino acids. One or two dCs were inserted opposite the dG-C8-PhIP adduct by this polymerase, and misinsertions of three other nucleotides were also observed to a certain extent (Fig. 6*B*). pol κ incorporated two dCs and misincorporated dG, dA, and dT into the A-p27 substrate without the PhIP adduct at a low efficiency (Fig. 6*A*). Misincorporations of dG, dA, and dT into the A-p28 substrate without the adduct were also observed (Fig. 6*C*). In the case of the extension reaction from 3′-dC opposite the dG-PhIP adduct, pol κ also incorporated dC and misincorporated dT into the C-p28 substrate at low efficiency (Fig. 6*D*). Interestingly, one- and two-base incorporations of dG into the substrate C-p28 by pol κ dominated the incorporation of a dC (Fig. 6*D*). In the extension reaction with pol κ in the presence of all four dNTPs, fragments of 29 and 30 nucleotides were observed as major products, and a small amount of the 31-nucleotide fragment was observed (see supplemental Fig. S5, *lane 6*). Full-length products of 32 nucleotides were observed only when an excess amount of pol κ was present (data not shown). This poor extension activity of pol κ after adding two nucleotides was probably caused by the shortness (~4 nucleotides) of the 5′ region to the lesion in the template oligonucleotide. Extension with pol κ, pol η, and pol δ from the mismatched primers, where the 3′-terminal nucleotide of the p28 primer, dC, was substituted with another nucleotide, could not be observed (data not shown). REV1 inserted a dC opposite the PhIP adduct at a higher efficiency compared with pol κ and pol η (Fig. 7, *B* and *C*). REV1 was, however, unable to catalyze the extension reaction from the dC opposite the PhIP adduct in C-p28 (Fig. 7*E* and supplemental Fig. S5, *lane 5*). REV1 incorporated only dC nucleotides into A-p27 and A-p28 substrates without the adduct (Fig. 7, *A* and *D*). Neither nucleotide insertion nor extension reactions for the templates containing the PhIP adduct were detected using human pol ι (data not shown).

Kinetic Analyses of Translesional DNA Synthesis by pol κ and REV1—To evaluate translesional DNA synthesis beyond the dG-C8-PhIP adduct in further detail, additional quantitative analyses for pol κ and REV1 were performed. Insertion reactions catalyzed by pol κ for dC (Fig. 8, *B*, *lanes 2–5*, and *C*, *closed diamonds*) and dG (Fig. 8, *B*, *lanes 6–9*, and *C*, *closed triangles*) into substrate C-p28 were analyzed in the same way. Kinetic parameters for pol κ were determined using steady-state kinetic assays (Table 2). The catalytic efficiency (k_{cat}/K_m) of dC insertion into C-p28 (0.039 min^{-1} mM^{-1}) was found to be 4-fold greater than that into C-p27 (0.011 min^{-1} mM^{-1}). These results indicate that pol κ catalyzes the extension reaction from the 3′-terminal of dC opposite the dG-C8-PhIP with a higher efficiency than the insertion reaction opposite the adduct. The k_{cat}/K_m values of the dC insertion opposite the adduct were roughly 4 orders of magnitude less than those into counterparts without the adduct (see Table 2). The k_{cat}/K_m value of the dG incorporation into C-p28 was slightly higher than that of dC, and more than 8-fold higher than that of dG into C-p27 (see Table 2). This result indicates that pol κ skipped over the dG site just 5′ of dG-C8-PhIP on the template and incorporated dG opposite dC on the template strand of substrate C-p28 with a high efficiency. The k_{cat}/K_m values of the dC incorporation into D-p27 (0.19 min^{-1} mM^{-1}) were over 4-fold greater than into C-p28 (0.039 min^{-1} mM^{-1}) and over 8-fold higher than that of dG into B-p29 (0.023) (see supplemental Table S1). These data indicate that the efficiencies of the extension reaction by pol κ are the highest for template p32D containing the PhIP adduct in the third G of the triple G run, next for template p32C containing the PhIP/adduct in the second G, and lowest for template p32B containing the PhIP adduct in the first G.

Even at higher concentrations of dNTPs, extension reactions catalyzed by REV1 for substrate C-p28 could not be monitored (Table 3, Fig. 7*E*). The k_{cat}/K_m value of the dC incorporation by REV1 into substrate C-p27 was more than 2,000 times greater than that by pol k, and 1/44 of the values for counterparts with-

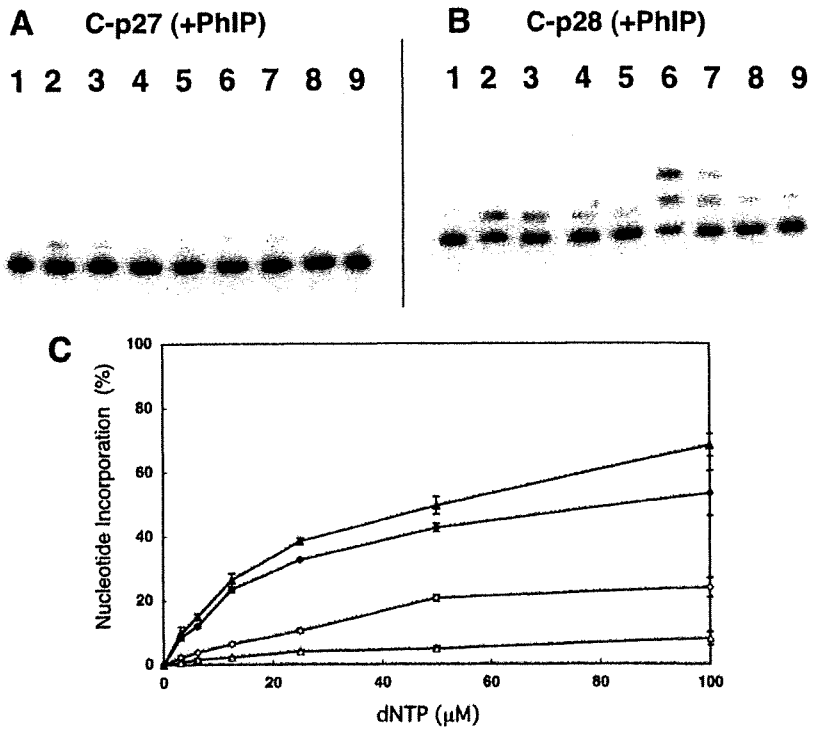

FIGURE 8. **Translesional DNA synthesis by pol κ.** Nucleotide incorporation by pol κ for substrates C-p27 (*A*) and C-p28 (*B*). Either dCTP (*lanes 2-5*) or dGTP (*lanes 6-9*) was added into the reaction mixture. *Lane 1* indicates a control without any nucleotides. The concentration of pol κ was 910 nM. The concentrations of dCTP or dGTP, respectively, were 25 (*lanes 2* and *6*), 12.5 (*lanes 3* and *7*), 6.25 (*lanes 4* and *8*), and 3.13 μM (*lanes 5* and *9*). *C*, incorporation efficiencies of dCTP and dGTP into substrate C-p27 and C-p28. Incorporations of dCTP into C-p27, dGTP into C-p27, dCTP into C-p28, and dGTP into C-p28 are indicated by *open diamonds*, *open triangles*, *closed diamonds*, and *closed triangles*, respectively. Each data point represents the mean of two separate experiments. The *error bars* represent residuals.

TABLE 2
k_{cat}/K_m values for pol κ

Substrate	K_m	k_{cat}	k_{cat}/K_m
	μM	$\times 10^{-3}$ min^{-1}	min^{-1} mM^{-1}
C-p27			
dCTP	70	0.76	0.011
dGTP	47	0.24	0.0050
C-p28			
dCTP	8.0	0.32	0.039
dGTP	11	0.48	0.042
A-p27			
dCTP	0.035	4.4	130
dGTP	0.26	1.3	5.0
A-p28			
dCTP	0.027	3.7	140
dGTP	2.1	8.8	4.1

TABLE 3
k_{cat}/K_m values for dCTP-insertion by REV1

Substrate	K_m	k_{cat}	k_{cat}/K_m
	μM	$\times 10^{-3}$ min^{-1}	min^{-1} mM^{-1}
C-p27	12	320	27
C-p28	ND[a]	ND	ND
A-p27	0.36	390	1100

[a] ND, not detectable.

out the adduct (Table 3). The k_{cat}/K_m values of the dC insertion by REV1 into three substrates, B-p28, C-p27 and D-p26, were 39, 27, and 73 min^{-1} mM^{-1}, respectively. Thus, the insertion reaction catalyzed by REV1 among the three templates was the most efficient for template p32D containing the PhIP adduct at the third G, similar to the extension reaction by pol κ.

DISCUSSION

In Vitro TLS Analysis Reconstituting PhIP-induced Mutations—HCAs are food-borne carcinogens produced when cooking meat (1, 9, 33). The most significant aspect of these molecules is that they exist normally in cooked food and are thus ubiquitous carcinogens (32). The mutagenicity and carcinogenicity of HCAs are mainly attributed to C8- and N2-dG adducts (9). Both excision repair and translesional DNA synthesis play critical roles in the mutagenesis steps induced by HCAs. However, despite the importance of HCAs as common environmental mutagens, there have been very few previous reports regarding the stalling of DNA polymerases and TLS caused by the DNA adducts they form. This is mainly because of the difficulty in preparing template DNA with introduced HCA adducts at specific sites. Choi *et al.* (34) have recently undertaken a biochemical study of TLS at adducts of the HCA 2-amino-3-methylimidazo[4,5-*f*]quinoline (IQ) using purified human polymerases. In our current study of TLS, we describe our findings for adducts of PhIP, the most abundant HCA in cooked foods (4).

A rat colon cancer model induced by PhIP shows profiles of cancer development similar to the multistep model of colon carcinogenesis in humans (35). In this rat model, *p53* and K-*ras* mutations are rarely observed, whereas mutations in *Apc* and its downstream gene *β-catenin* have been frequently observed (21, 36–38). Hence, mutations in *Apc* or *β-catenin* have been speculated to play a critical role in PhIP-induced colon carcinogenesis. Five mutations in the *Apc* gene were previously detected in four of eight PhIP-induced rat colon tumors, and all of these mutations involved a single guanine deletion in the 5′-GGGA-3′ sequence (21). This characteristic mutation induced by PhIP, 5′-GGGA-3′ to 5′-GGA-3′, was also observed in other *in vivo* mutation analyses using transgenic animals harboring introduced reporter genes, such as *lacI* (18–20). Hence, the 5′-TCCGGGAAC-3′ sequence corresponding to a mutation hot spot within the rat *Apc* gene, which we utilized to introduce the PhIP adduct and employed as the template for *in vitro* DNA synthesis analyses, could be a suitable model for revealing the molecular mechanisms associated with PhIP-induced mutations.

As discussed later, our results indicate a possible molecular mechanism for the 5′-GGGA-3′ to 5′-GGA-3′ mutation induced by PhIP.

DNA Polymerases Involved in TLS through the dG-PhIP Adduct—TLS through many DNA lesions requires the action of two different polymerases, an "inserter" and an "extender," the former to perform nucleotide insertions opposite the lesion site and the latter for subsequent extensions (39). The catalytic efficiency of the dCTP-insertion reaction opposite the dG-PhIP adduct by REV1 was found to be more than 2,000-fold greater than that by pol κ (see Tables 2 and 3). This result strongly suggests that REV1 functions *in vivo* as an inserter polymerase for TLS through the dG-PhIP adduct. This insertion step by REV1 is also error free. REV1 has been reported previously to insert dCTP opposite abasic sites and various N2-dG adducts (26, 39–41). However, our current study is the first to show that REV1 inserts dCTP opposite a large size C8-dG adduct. We used a shorter (C-terminal deleted) form of pol κ in our current experiments and an intact pol κ may be more effective for this insertion reaction. As for pol η, a detailed kinetic analysis was not performed. Hence, the possibility cannot be excluded that pol κ and pol η also function as inserter polymerases.

In addition to the Y-family DNA polymerases, DNA polymerase ζ (pol ζ), belonging to the B-family DNA polymerases, is considered to be involved in TLS through various lesions as an extender DNA polymerase (39, 42, 43). We have not carried out a primer extension assay with pol ζ and thus the possibility cannot be completely excluded by our current data that pol ζ functions *in vivo* as an extender polymerase for TLS through the dG-PhIP adduct. In our present study, we provide evidence that pol κ can extend from dC opposite the dG-C8-PhIP adduct *in vitro*. It is, therefore, possible that pol κ, at least partially, functions as an extender polymerase *in vivo* for TLS through the dG-PhIP adduct. Further study about cooperation between two or more DNA polymerases, including pol ζ, is necessary to verify which DNA polymerases are involved in the bypass synthesis through the PhIP lesion.

The catalytic efficiency of pol κ for a dGTP insertion into substrate C-p28 was a little higher than that for dCTP insertions (see Table 2 and Fig. 6*D*). The former generates a single guanine deletion, and the latter is an error-free extension. Consequently, our data suggest that the extension reaction with pol κ from the nucleotide opposite the dG-C8-PhIP adduct causes frequent single-guanine deletions from the GGG stretch. It has been reported that one characteristic feature of pol κ homologs, from bacteria to humans, is their propensity to generate single-base deletions (44–47). The crystal structure of Dpo4, a thermophilic archaea homolog of pol κ, in ternary complexes with DNA and an incoming nucleotide supports the model that a single base deletion by pol κ is generated through a misaligned intermediate complex where the template dG forms an extrahelical looped out structure and the incoming dGTP skips this extrahelical base and pairs with the next template base dC (48) (see supplemental Fig. S6). It is reasonable to speculate therefore that, in the case of TLS through dG-C8-PhIP, mammalian pol κ generates the single guanine deletion via a similar intermediate where the PhIP-adducted dG is looped out and template-primer slippage occurs. However, further analyses for determining whether the one-base skipping of pol κ beyond the lesion observed by us is dependent on the nucleotide placed 5′ to the lesion or not, are necessary to clarify the detailed molecular mechanism underlying one base skipping of pol κ.

Molecular Mechanisms Underlying Mutation Induction by PhIP—We have demonstrated herein by *in vitro* DNA synthesis analyses using oligonucleotide templates containing dG-PhIP that: 1) replicative DNA polymerases stall at the PhIP adduct and cannot perform translesional DNA synthesis beyond this point; 2) REV1 inserts a dC opposite the dG-PhIP with a much higher efficiency than other TLS polymerases, including pol κ and pol η; and 3) pol κ has a potential ability to catalyze an extension reaction from the 5′-dC opposite the adduct and often skips over one dG in the template during this extension step. A working model for the induction of mutations at the PhIP adducts based on the results shown in the present study is illustrated in supplemental Fig. S6. This model could be adopted for other sequences containing a G repeat stretch longer than GGG.

REFERENCES

1. Nagao, M. (2000) in *Food Borne Carcinogens: Heterocyclic Amines* (Nagao, M., and Sugimura, T., eds) pp. 163–196, John Wiley & Sons Ltd., Chichester, UK
2. Schut, H. A., and Snyderwine, E. G. (1999) *Carcinogenesis* **20,** 353–368
3. Felton, J. S., Knize, M. G., Shen, N. H., Lewis, P. R., Andresen, B. D., Happe, J., and Hatch, F. T. (1986) *Carcinogenesis* **7,** 1081–1086
4. Felton, J. S., Jagerstad, M., Knize, M. G., Skog, K., and Wakabayashi, K. (2000) in *Food Borne Carcinogens: Heterocyclic Amines* (Nagao, M., and Sugimura, T., eds) pp. 31–71, John Wiley & Sons Ltd., Chichester, UK
5. Holme, J. A., Wallin, H., Brunborg, G., Søderlund, E. J., Hongslo, J. K., and Alexander, J. (1989) *Carcinogenesis* **10,** 1389–1396
6. Felton, J. S., and Knize, M. G. (1991) *Mutat. Res.* **259,** 205–217
7. Ohgaki, H., Takayama, S., and Sugimura, T. (1991) *Mutat. Res.* **259,** 399–410
8. Ito, N., Hasegawa, R., Sano, M., Tamano, S., Esumi, H., Takayama, S., and Sugimura, T. (1991) *Carcinogenesis* **12,** 1503–1506
9. Sugimura, T., Wakabayashi, K., Nakagama, H., and Nagao, M. (2004) *Cancer Sci.* **95,** 290–299
10. Imaida, K., Hagiwara, A., Yada, H., Masui, T., Hasegawa, R., Hirose, M., Sugimura, T., Ito, N., and Shirai, T. (1996) *Jpn. J. Cancer Res.* **87,** 1116–1120
11. Frandsen, H., Grivas, S., Andersson, R., Dragsted, L., and Larsen, J. C. (1992) *Carcinogenesis* **13,** 629–635
12. Lin, D., Kaderlik, K. R., Turesky, R. J., Miller, D. W., Lay, J. O., Jr., and Kadlubar, F. F. (1992) *Chem. Res. Toxicol.* **5,** 691–697
13. Snyderwine, E. G., Davis, C. D., Nouso, K., Roller, P. P., and Schut, H. A. (1993) *Carcinogenesis* **14,** 1389–1395
14. Schut, H. A., and Herzog, C. R. (1992) *Cancer Lett.* **67,** 117–124
15. Endo, H., Schut, H. A., and Snyderwine, E. G. (1994) *Cancer Res.* **54,** 3745–3751
16. Morgenthaler, P. M., and Holzhäuser, D. (1995) *Carcinogenesis* **16,** 713–718
17. Yadollahi-Farsani, M., Gooderham, N. J., Davies, D. S., and Boobis, A. R. (1996) *Carcinogenesis* **17,** 617–624
18. Okonogi, H., Stuart, G. R., Okochi, E., Ushijima, T., Sugimura, T., Glickman, B. W., and Nagao, M. (1997) *Mutat. Res.* **395,** 93–99
19. Lynch, A. M., Gooderham, N. J., Davies, D. S., and Boobis, A. R. (1998) *Mutagenesis* **13,** 601–605
20. Okochi, E., Watanabe, N., Shimada, Y., Takahashi, S., Wakazono, K., Shirai, T., Sugimura, T., Nagao, M., and Ushijima, T. (1999) *Carcinogenesis* **20,** 1933–1988
21. Kakiuchi, H., Watanabe, M., Ushijima, T., Toyota, M., Imai, K., Weisburger, J. H., Sugimura, T., and Nagao, M. (1995) *Proc. Natl. Acad. Sci.*

U.S.A. **92,** 910–914
22. Takamura-Enya, T., Ishikawa, S., Mochizuki, M., and Wakabayashi, K. (2006) *Chem. Res. Toxicol.* **19,** 770–778
23. Masuda, Y., Suzuki, M., Piao J., Gu, Y., Tsurimoto, T., and Kamiya, K. (2007) *Nucleic Acids Res.* **35,** 6904–6916
24. Masutani, C., Kusumoto, R., Iwai, S., and Hanaoka, F. (2000) *EMBO J.* **19,** 3100–3109
25. Niimi, N., Sassa, A., Katafuchi, A., Grúz, P., Fujimoto, H., Bonala, R. R., Johnson, F., Ohta, T., and Nohmi, T. (2009) *Biochemistry* **48,** 4239–10234246
26. Masuda, Y., and Kamiya, K. (2002) *FEBS Lett.* **520,** 88–92
27. Masuda, Y., Ohmae, M., Masuda, K., and Kamiya, K. (2003) *J. Biol. Chem.* **278,** 12356–12360
28. Sambrook, J., Fritsch, E. F., and Maniatis, T. (1989) *Molecular Cloning: A Laboratory Manual,* 2nd Ed., Cold Spring Harbor Laboratory, Cold Spring Harbor, NY
29. Fukuda, H., and Ohtsubo, E. (1997) *Genes Cells* **2,** 735–751
30. Fukuda, H., Katahira, M., Tsuchiya, N., Enokizono, Y., Sugimura, T., Nagao, M., and Nakagama, H. (2002) *Proc. Natl. Acad. Sci. U.S.A.* **99,** 12685–12690
31. Sugiyama, H., and Saito, I. (1996) *J. Am. Chem. Soc.* **118,** 7063–7068
32. Mozzherin, D. J., Shibutani, S., Tan, C. K., Downey, K. M., and Fisher, P. A. (1997) *Proc. Natl. Acad. Sci. U.S.A.* **94,** 6126–6231
33. Sugimura, T., and Adamson, R. H. (2000) in *Food Borne Carcinogens: Heterocyclic Amines* (Nagao, M., and Sugimura, T., eds) pp. 1–4, John Wiley & Sons Ltd., Chichester, UK
34. Choi, J. Y., Stover, J. S., Angel, K. C., Chowdhury, G., Rizzo, C. J., and Guengerich, F. P. (2006) *J. Biol. Chem.* **281,** 25297–25306
35. Nakagama, H., Ochiai, M., Ubagai, T., Tajima, R., Fujiwara, K., Sugimura, T., and Nagao, M. (2002) *Mutat. Res.* **506–507,** 137–144
36. Nagao, M. (1999) *Mutat. Res.* **431,** 3–12
37. Nagao, M., Ushijima, T., Toyota, M., Inoue, R., and Sugimura, T. (1997) *Mutat. Res.* **376,** 161–167
38. Dashwood, R. H., Suzui, M., Nakagama, H., Sugimura, T., and Nagao, M. (1998) *Cancer Res.* **58,** 1127–1129
39. Prakash, S., Johnson, R. E., and Prakash, L. (2005) *Annu. Rev. Biochem.* **74,** 317–353
40. Nelson, J. R., Lawrence, C. W., and Hinkle, D. C. (1996) *Nature* **382,** 729–731
41. Haracska, L., Prakash, S., and Prakash, L. (2002) *J. Biol. Chem.* **277,** 15546–15551
42. Johnson, R. E., Washington, M. T., Haracska, L., Prakash, S., and Prakash, L. (2000) *Nature* **406,** 1015–1019
43. Haracska, L., Unk, I., Johnson, R. E., Johansson, E., Burgers, P. M., Prakash, S., and Prakash, L. (2001) *Genes Dev.* **15,** 945–954
44. Kim, S. R., Maenhaut-Michel, G., Yamada, M., Yamamoto, Y., Matsui, K., Sofuni, T., Nohmi, T., and Ohmori, H. (1997) *Proc. Natl. Acad. Sci. U.S.A.* **94,** 13792–13797
45. Kobayashi, S., Valentine, M. R., Pham, P., O'Donnell, M., and Goodman, M. F. (2002) *J. Biol. Chem.* **277,** 34198–34207
46. Ogi, T., Kato, T., Jr., Kato, T., and Ohmori, H. (1999) *Genes Cells* **4,** 607–618
47. Ohashi, E., Bebenek, K., Matsuda, T., Feaver, W. J., Gerlach, V. L., Friedberg, E. C., Ohmori, H., and Kunkel, T. A. (2000) *J. Biol. Chem.* **275,** 39678–39684
48. Ling, H., Boudsocq, F., Woodgate, R., and Yang, W. (2001) *Cell* **107,** 91–102

Published online 29 April 2009

Nucleic Acids Research, 2009, Vol. 37, No. 12 3959–3968
doi:10.1093/nar/gkp262

The ATR-Chk1 pathway plays a role in the generation of centrosome aberrations induced by Rad51C dysfunction

Mari Katsura[1,2], Takanori Tsuruga[2], Osamu Date[2], Takashi Yoshihara[2], Mari Ishida[2], Yoshitaka Tomoda[1], Miyuki Okajima[1], Motoki Takaku[3], Hitoshi Kurumizaka[3], Aiko Kinomura[2], Hiromu K. Mishima[4] and Kiyoshi Miyagawa[1,2,*]

[1]Laboratory of Molecular Radiology, Center for Disease Biology and Integrative Medicine, Graduate School of Medicine, The University of Tokyo, 7-3-1 Hongo, Bunkyo-ku, Tokyo 113-0033, [2]Department of Human Genetics, Research Institute for Radiation Biology and Medicine, Hiroshima University, 1-2-3 Kasumi, Minami-ku, Hiroshima 734-8553, [3]Laboratory of Structural Biology, Graduate School of Advanced Science and Engineering, Waseda University, 2-2 Wakamatsu-cho, Shinjuku-ku, Tokyo 162-8480 and [4]Department of Ophthalmology, Graduate School of Medical Sciences, Hiroshima University, 1-2-3 Kasumi, Minami-ku, Hiroshima 734-8553, Japan

Received September 4, 2008; Revised March 6, 2009; Accepted April 8, 2009

ABSTRACT

Rad51C is a central component of two complexes formed by five Rad51 paralogs in vertebrates. These complexes are involved in repairing DNA double-strand breaks through homologous recombination. Despite accumulating evidence suggesting that the paralogs may prevent aneuploidy by controlling centrosome integrity, Rad51C's role in maintaining chromosome stability remains unclear. Here we demonstrate that Rad51C deficiency leads to both centrosome aberrations in an ATR-Chk1-dependent manner and increased aneuploidy in human cells. While it was reported that Rad51C deficiency did not cause centrosome aberrations in interphase in hamster cells, such aberrations were observed in interphase in HCT116 cells with Rad51C dysfunction. Caffeine treatment and down-regulation of ATR, but not that of ATM, reduced the frequency of centrosome aberrations in the mutant cells. Silencing of Rad51C by RNA interference in HT1080 cells resulted in similar aberrations. Treatment with a Chk1 inhibitor and silencing of Chk1 also reduced the frequency in HCT116 mutants. Accumulation of Chk1 at the centrosome and nuclear foci of γH2AX were increased in the mutants. Moreover, the mutant cells had a higher frequency of aneuploidy. These findings indicate that the ATR-Chk1 pathway plays a role in increased centrosome aberrations induced by Rad51C dysfunction.

INTRODUCTION

Homologous recombination, along with nonhomologous end-joining, plays a major role in the repair of DNA double-stranded breaks (DSBs) (1). Rad51 is a key player in homologous recombination by exerting homologous pairing and strand exchange activities. Rad51 paralogs are assumed to be involved in the early stages of homologous recombination by assisting Rad51 function (2). Five members of the Rad51 paralog family constitute two protein complexes: Rad51B-Rad51C-Rad51D-XRCC2 (BCDX2) and Rad51C-XRCC3 (3,4). Thus, Rad51C is a central component among five members in vertebrates.

The centrosome serves as the microtubule-organizing center, ensuring correct chromosome segregation to prevent aneuploidy (5). Accumulating evidence suggests that centrosome dysfunction, typically represented by abnormal numbers of centrosomes, is involved in human diseases, particularly in cancers (6). More than 100 proteins have been reported to be localized in the centrosome (7). Deletion of these proteins often leads to centrosome aberrations.

Mutations of XRCC2, XRCC3, Rad51B and Rad51D were shown to increase centrosome fragmentation and aneuploidy (8–10). Despite these observations, the role of Rad51C in the maintenance of centrosome integrity and chromosome stability remains unclear. Initially, Rad51C-deficient Chinese hamster ovary (CHO) cells, CL-V4B, were shown to exhibit no increase in centrosome aberrations (11). A recent study, however, demonstrated that centrosome numbers were increased only in mitosis and not in interphase in CL-V4B cells (12).

*To whom correspondence should be addressed. Tel: +81 358413503; Fax: +81 358413013; Email: miyag-tky@umin.ac.jp

Moreover, although increased numbers of centrosomes are assumed to generate aneuploidy, no studies using mammalian cells have demonstrated that Rad51C deficiency leads to increased aneuploidy.

The mechanisms underlying centrosome aberrations observed in cells with a defect in homologous recombination are controversial. In chicken DT40 cells with a conditional mutation of Rad51, the ATM-dependent checkpoint pathway was proposed to be responsible for centrosome amplification at the G2 phase (13). However, the results of a study using CHO cells with the dominant-negative Rad51 protein argued against this result (14). The hereditary breast cancer susceptibility protein BRCA1 is also involved in homologous recombination. Recent evidence suggests that HMMR, encoding the hyaluronan-mediated motility receptor, is a substrate of BRCA1-BARD1 E3 ubiquitin ligase activity and plays a role in centrosomal function (15).

Supernumerary centrosomes induced by ionizing radiation were shown to be caused by the Chk1-mediated pathway, indicating that the DNA damage response signal is involved in centrosome amplification (16). Treatment with caffeine, an inhibitor of ATM and ATR kinases, reduced centrosome amplification induced by ionizing radiation, suggesting that either or both kinases may be involved in centrosome amplification. However, caffeine treatment in ATM- or ATR-deficient cells also reduced centrosome amplification. Thus, the roles of ATM and ATR in promoting centrosome amplification induced by ionizing radiation appear to be complementary.

To investigate Rad51C's role in the maintenance of chromosome stability, we knocked out the gene in the human colon cancer cell line HCT116. We also silenced the gene by RNA interference in the human fibrosarcoma cell line HT1080. Supernumerary centrosomes in these cells with Rad51C dysfunction were increased at both interphase and metaphase in an ATR-Chk1-dependent manner. Consistent with this observation, aneuploidy was increased in HCT116 cells with Rad51C dysfunction. Our observations suggest that the ATR-Chk1 pathway plays a role in increased centrosome aberrations induced by Rad51C dysfunction in human cancer cells.

MATERIALS AND METHODS

Cell culture

HCT116 cells were cultured in McCoy's 5A medium supplemented with 10% fetal bovine serum (FBS). HT1080 cells were cultured in the minimum essential medium Eagle (MEM) supplemented with 10% FBS. These cells were obtained from the American Type Culture Collection. 2-Morpholin-4-yl-6-thianthren-1-yl-pyran-4-one (KU55933) and 7-hydroxystaurosporine (UCN-01) were purchased from Merck Calbiochem.

Generation of Rad51C mutant cells

The 8-kb left arm and 1.5-kb right arm of the *RAD51C* genomic fragments were isolated from the EMBL3 SP6/T7 human genomic library (Clontech) and inserted into pBluescript SK for neomycin and blasticidin selection. The shorter genomic fragment was isolated from the genomic DNA of HCT116 by PCR amplification for puromycin selection. The 2.4-kb left arm was amplified using primers 5′-TTTGGCTGCTCCGGGGTTA-3′ and 5′-CAGAGTTTCTAAGGCTTCTGC-3′. The 1.5-kb right arm was amplified using primers 5′-CTCGAGTGGAGTGCCCTTAAT-3′ and 5′-CTCGAGTCAACAGAAAGATGAC-3′. Promoterless neomycin-, blasticidin- and puromycin-resistant genes were inserted into the Dra I site in exon 2. Gene targeting in HCT116 was carried out as previously described (17).

Complementation experiments

The *RAD51C* cDNA was amplified from normal human cDNA using primers 5′-TTTGGCTGCTCCGGGGTTA-3′ and 5′-CATTCATGCCATAGTGTG-3′, and cloned into pCR2.1 (Invitrogen) by the TA cloning method. After the sequence was confirmed, the cDNA was inserted into an expression vector under the control of the MSV enhancer and the MMTV promoter. The generation of the XRCC3 expression vector has been described earlier (18).

Sensitivity to DNA-damaging agents

After 1×10^3 cells were cultured in a 60 mm dish for 24 h, they were exposed to mitomycin C (MMC) (Kyowa Hakko Kogyo) for 10 min, hydroxyurea (HU) (Sigma-Aldrich) for 24 h or γ-ray irradiation. They were further cultured for 9 days, and the colonies were counted.

Sister chromatid exchange (SCE) and gene targeting frequency

SCEs were analyzed essentially as previously described (17). Cells were cultured in 16 μM 5-bromodeoxyuridine (BrdU) for 36 h (wild type), 42 h (*RAD51C*$^{+/-/-/-}$) or 41 h (*RAD51C*$^{+/-/-/-}$ + cDNA), and pulsed with 0.1 μg/ml colcemid for the last 1 h. To examine the effect of MMC, cells were incubated in the presence of 0.8 μg/ml MMC for 8 h before harvest. Harvested cells were treated with 75 mM KCl:1% sodium citrate (4:1) for 20 min and fixed with methanol:acetic acid (3:1). Cells were fixed on slides and incubated with 12.8 μg/ml Hoechst 33258 for 20 min. The slides were irradiated with ultraviolet for 1 h at 60°C and stained with Giemsa solution. Gene targeting frequencies at the *RAD54B* locus were examined as previously described (17).

Antibodies

Anti-ATM (5C2), ATR (N-19), Chk1 (G-4 and DCS-310) and Cdk2 (M2) antibodies were from Santa Cruz Biotechnology. Anti-γ-tubulin (T3559 and T6557) and β-actin (A1978) antibodies were from Sigma-Aldrich. The anti-XRCC3 antibody (NB100-165) was from Novus Biologicals. Anti-phospho-H2AX Ser 139 (07-164) and Chk2 (05-649) antibodies were from Upstate Biotechnology. The anti-Chk2 antibody (DCS-273) was from Medical & Biological Laboratories. The anti-Rad51B antibody was obtained from rabbits immunized with the recombinant Rad51B protein (19). The anti-Rad51C antibody (ab3669) was from Abcam.

Immunofluorescence

Cells grown on coverslips were fixed for 10 min in 4% paraformaldehyde. Then, they were permeabilized with 0.5% Triton X-100 and 0.1% SDS/PBS for 5 min. Cells were blocked with 10% horse serum at 4°C for 30 min and incubated with primary antibodies at 37°C for 1 h and with secondary antibodies for 30 min. Finally, cells were counterstained with 4′,6′-diamidino-2-phenylindole (DAPI) and mounted. Slides were analyzed using Olympus BX51-DP70, Carl Zeiss AxioImagerZ1/Apotome and Nikon Confocal Laser Microscope system A1.

Fluorescence *in situ* hybridization analysis

Chromosome-specific centromeric probes were obtained from Vysis. DNA in cells was denatured in 70% formamide/2× SSC at 73°C for 5 min. Hybridization was performed in a CEP hybridization buffer (Vysis) at 42°C for 1 h. Slides were washed in 0.4× SSC/0.3% NP40 at 73°C for 2 min and in 2× SSC/0.1% NP40 at room temperature for 1 min. Cellular DNA was stained with DAPI.

RNA interference

siCONTROL, Rad51C siGENOME set of 4, ATM SMARTpool, ATR SMARTpool, Chk1 SMARTpool and Chk2 SMARTpool small interference RNAs (siRNAs) were purchased from Dharmacon. Cells were transfected with 100 nM siRNA and Dharmafect4 (Dharmacon) according to the manufacturer's instructions. Cells were harvested at 72 h post-transfection.

Cell-cycle analysis

Cells treated with siRNAs were harvested 72 h after transfection. EPICS XL (Beckman Coulter) was used for cell-cycle analysis.

Kinase assay

Cells were dissolved into a lysis buffer (50 mM Tris–HCl pH 7.5, 150 mM NaCl, 1% Nonidet P40, 10% glycerol and 2 mM EDTA) containing phosphatase inhibitors (50 nM cantharidin, 5 nM microcystin and 25 mM bromotetramisole oxalate), 2 mg/ml aprotinin and 0.5 mM PMSF for 15 min on ice and lysed by sonication. After centrifugation (12 000 rpm, 5 min), the supernatant was collected and precleared by incubation with normal IgG for 1 h and Protein G for 30 min. Precleared lysate was incubated with anti-Chk1 or anti-Chk2 antibody for 1 h. After incubation with Protein G, immunoprecipitates were washed three times each with the lysis buffer and 25 mM Hepes. The washed precipitate was incubated in a kinase reaction buffer (25 mM Hepes pH 7.4, 15 mM $MgCl_2$, 80 mM EGTA and 1 mM DTT) with 0.1 mM ATP, 3 μCi[γ-^{32}P]ATP and 10 μg glutathione *S*-transferase (GST)-Cdc25C (200–256) at 30°C for 30 min. The reaction was stopped by the addition of the sample buffer and subjected to SDS-PAGE. GST-Cdc25C (200–256) was prepared as previously described (20).

RESULTS

Rad51C is involved in homologous recombination in human cells

To investigate the role of Rad51C in human cells, the gene was sequentially knocked out in HCT116 cells (Figure 1A). In accordance with the finding that *RAD51C* was frequently amplified in human cancer cells, Southern blot analysis demonstrated that this cell line harbors four alleles of the gene (Figure 1B) (21,22). Two independent *RAD51C*$^{+/-/-/-}$ cell lines (#1 and #2) were isolated. The levels of Rad51C expression in proportion to targeting events were confirmed by northern and western blot analyses (Figure 1C and D). These cells were used in function analysis as Rad51C mutant cells because clear phenotypes indicating defective homologous recombination in comparison with wild-type HCT116 cells were observed. Complementation experiments were performed using cells transfected with the exogenous Rad51C expression vector.

The mean of the frequency of SCE induced by MMC per cell was 5.8 in the Rad51C mutant cells, a value that was significantly lower than 8.3, the mean value for wild-type cells (Table 1). The SCE frequency increased to a level comparable to that of the wild-type cells in cells transfected with the Rad51C expression vector. Gene targeting frequency was examined at the *RAD54B* locus, because it was assumed that Rad54B is not functionally related to Rad51C (17). The frequency in the Rad51C mutant cells was 1.16%, which was significantly lower than 12.0%, the wild-type value. These results indicate that Rad51C plays a role in homologous recombination, a finding that is in accord with the observations in DT40, CHO and HeLa cells (11,12,23,24).

Homologous recombination is required for the repair of DSBs induced by DNA-damaging agents. The Rad51C mutant cells were hypersensitive to ionizing radiation, MMC and HU, which was complemented by the exogenous expression of the gene, indicating that Rad51C plays a role in DSB repair (Figure 2A–C). A defect in homologous recombination leads to an increase in chromosome aberrations such as gaps and breaks. Giemsa staining using a metaphase spread revealed that both chromosome- and chromatid-type aberrations were increased in Rad51C mutant cells, indicating that spontaneously arising DSBs were not properly repaired (Table 2). These observations suggest that Rad51C plays a role in the repair of DSB through homologous recombination in human cells.

Rad51C dysfunction leads to increased centrosome aberrations

Since Rad51C's role in maintaining centrosome integrity has been controversial (11,12), we examined centrosome aberrations by immunostaining γ-tubulin. Cells with more than two centrosomes are observed more frequently in two independent Rad51C mutant clones than in wild-type cells (Figure 3A). The frequency of aberrant numbers of interphase centrosomes (more than two) was 7.0% in wild-type cells, whereas it was 28.0% (#1) and 30.3% (#2) in the Rad51C mutant cells. *RAD51C* cDNA expression

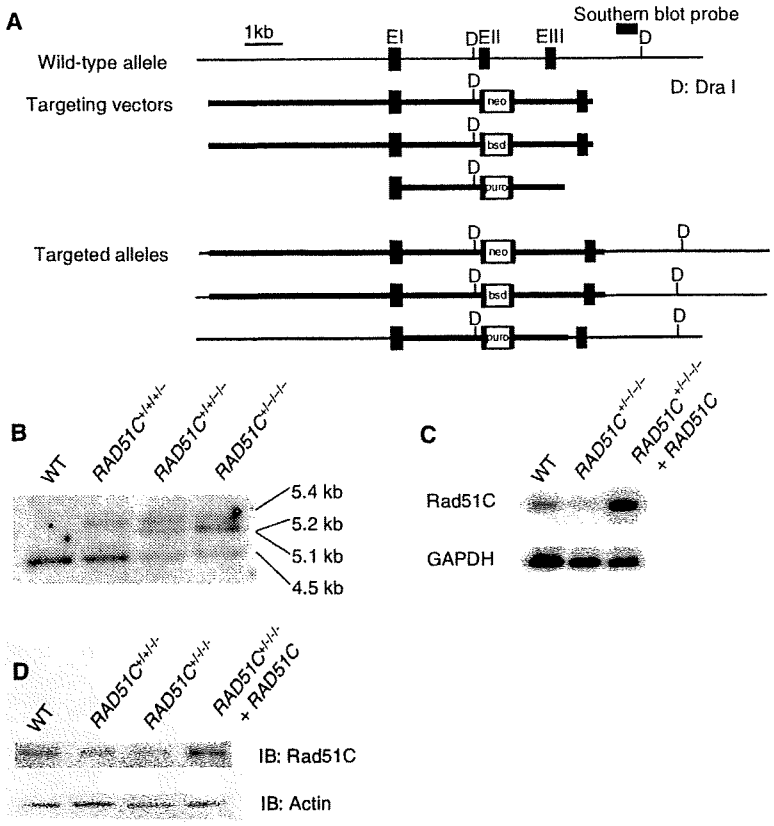

Figure 1. Generation of Rad51C mutant cells by gene targeting. **(A)** Strategy for gene targeting at the *RAD51C* locus. The targeting vectors, restriction sites and the position of the probe used for the Southern blot analysis are shown. **(B)** Southern blot analysis of DNA digested with Dra I. The size of the wild-type allele is 4.5 kb. Insertion of drug-resistance genes changes the size to 5.1, 5.2 and 5.4 kb. **(C)** Northern blot analysis of polyadenylated RNAs hybridized with the full-length *RAD51C* cDNA. **(D)** Western blot analysis. The Rad51C protein was immunoprecipitated with the rabbit polyclonal antibody and visualized by western blot analysis using the mouse monoclonal antibody.

Table 1. Sister chromatid exchanges and targeting frequency

Cell line	SCEs per cell[a]		Targeted integration[b]
	Spontaneous	MMC-induced	*RAD54B-hygro*
RAD51C$^{+/+/+/+}$	4.2 ± 0.2	8.3 ± 0.4	12.0% (13/108)
RAD51C$^{+/-/-/-}$	4.3 ± 0.3	5.8 ± 0.3[c]	1.16% (1/86)[d]
RAD51C$^{+/-/-/-}$ + cDNA	5.0 ± 0.2	8.2 ± 0.4	N.D.[e]

[a]Number of SCEs per cells represents the mean ± SEM from 100 mitotic cells.
[b]The frequency of targeted integration is shown as a percentage of the targeted clones relative to the total number of hygromycin resistant clones; the numbers of clones are given in parentheses.
[c]$P < 1.0 \times 10^{-4}$, based on Mann–Whitney U-tests, comparing wild-type cells with *RAD51C*$^{+/-/-/-}$ cells.
[d]$P = 0.0025$, based on Fisher's exact tests, comparing wild-type cells with *RAD51C*$^{+/-/-/-}$ cells.
[e]N.D., not determined.

in the mutant cells reduced the frequency to 16.3% (#2). In mitosis, the frequency was 8.0% in wild-type cells, and 24.0% (#1) and 32.8% (#2) in the mutant cells. cDNA expression in the mutant cells reduced the frequency to 21.5% (#2). Thus, unlike CHO cells with Rad51C mutation, in which centrosome aberrations were observed only at mitosis, the corresponding HCT116 cells demonstrated centrosome aberrations at both interphase and mitosis.

To confirm that a reduction in Rad51C levels leads to centrosome aberrations in other human cells, we silenced the gene in HT1080 cells by RNA interference. Western blot analysis showed that Rad51C expression was not altered in wild-type HT1080 cells and was reduced in the cells transfected with Rad51C siRNA (Figure 3B). The frequency of aberrant numbers of interphase centrosomes was 4.6% in cells transfected with control siRNA, whereas it was 9.1% in cells transfected with Rad51C siRNA (Figure 3C). Thus, supernumerary centrosomes were also increased in HT1080 cells with Rad51C dysfunction.

Rad51C affects XRCC3 levels

Since Rad51C is a central component of protein complexes formed by Rad51 paralogs, we investigated the effect of Rad51C dysfunction on the BCDX2 and Rad51C-XRCC3 complexes by measuring levels of

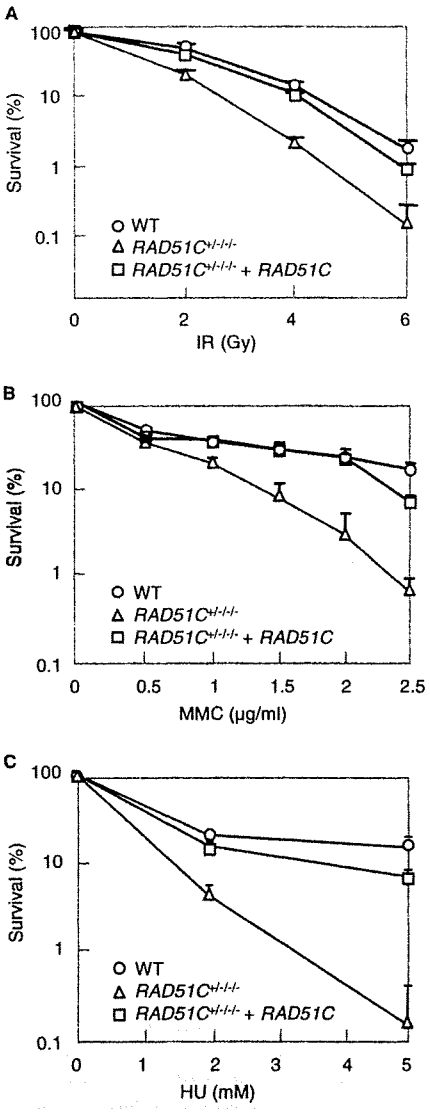

Figure 2. Sensitivity to DNA-damaging agents. **(A)** Sensitivity to ionizing radiation. **(B)** Sensitivity to MMC. **(C)** Sensitivity to HU. In (A), (B) and (C), the results represent the means ± SD of three experiments.

Table 2. Spontaneous chromosomal aberrations

Cell line	Chromatid type	Chromosome type	Abnormal cells
RAD51C$^{+/+/+/+}$	2	3	3
RAD51C$^{+/-/-/-}$	12	7	17
RAD51C$^{+/-/-/-}$ + cDNA	4	4	7

A total of 100 cells were scored for each cell line.

Rad51B and XRCC3. Western blot analysis revealed that XRCC3 levels but not Rad51B levels were reduced in the mutant cells (Figure 4A). The previous report that XRCC3 was destabilized in Rad51C-deficient human

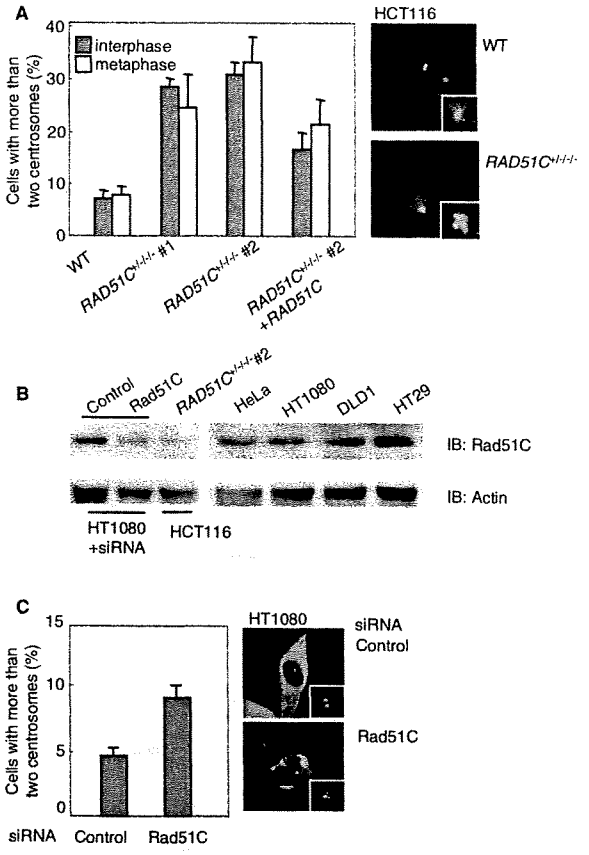

Figure 3. Centrosome aberrations. **(A)** Centrosome aberrations in HCT116 cells. For each clone at interface and metaphase, 100 cells and 50 cells, respectively, stained with the anti-γ-tubulin antibody by immunofluorescence were counted. **(B)** Western blot analysis showing the expression of Rad51C in HT1080 cells treated with either control or Rad51C siRNA. Rad51C levels in human cells are also shown as controls. **(C)** Centrosome aberrations in HT1080 cells. Cells were treated with either control or Rad51C siRNA and stained with the anti-γ-tubulin antibody. For each siRNA treatment at interface, 100 cells were counted. In (A) and (C), the results represent the means ± SEM of three independent experiments.

cells is in accord with this finding (24). Next, we investigated the effect of reduced XRCC3 levels on centrosome aberrations by expressing the *XRCC3* cDNA in the Rad51C mutant cells (Figure 4B and C). The frequency of centrosome aberrations was not changed by stable expression of XRCC3. Thus, centrosome aberrations induced by Rad51C dysfunction are unlikely to result from the destabilization of other Rad51 paralogs.

ATR is involved in promoting centrosome aberrations

We next examined the roles of ATM and ATR in centrosome aberrations in Rad51C mutant cells by a treatment with 2 mM caffeine (Figure 5A). FACS analysis confirmed that caffeine treatment at this concentration did not affect cell-cycle progression (data not shown). This treatment reduced the frequency of centrosome aberrations in the

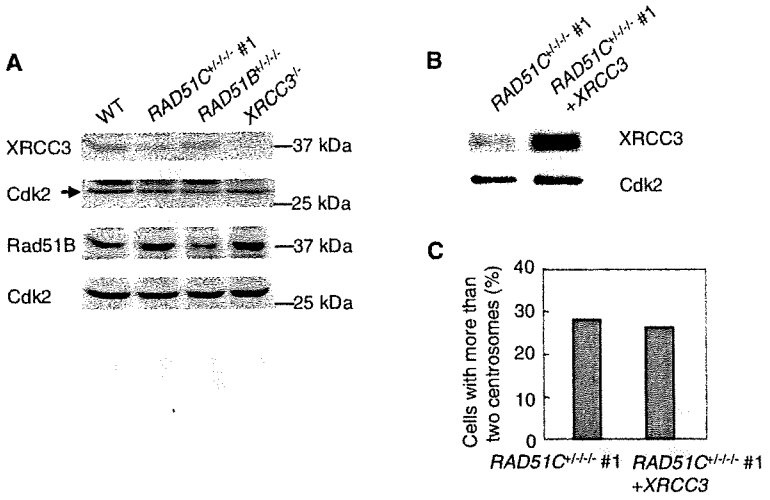

Figure 4. Effect of Rad51C dysfunction on levels of other Rad51 paralogs. (**A**) Expression of XRCC3 and Rad51B in Rad51C mutant cells. (**B**) Exogenous expression of XRCC3 in the mutant cells. (**C**) Effect of complementation of XRCC3 on centrosome aberrations in the mutant cells. A total of 200 cells were counted.

mutant from 29.0% to 15.8% ($P < 0.01$, paired t-test), indicating that ATM and/or ATR may be involved in the generation of supernumerary centrosomes.

ATM's effect on the centrosomes was examined by treatment with the ATM-specific inhibitor, KU55933 (Figure 5B). This treatment did not change the frequency of supernumerary centrosomes, indicating that ATM was not involved in the damage-dependent increase in supernumerary centrosomes. Next, the effects of ATM and ATR on the centrosomes were examined by using RNA interference to silence the genes. Western blot analysis demonstrated that each protein was down-regulated by RNA interference (Figure 5C). Treatment with ATM siRNA slightly affected the cell-cycle distribution of the mutant cells, whereas treatment with ATR siRNA did not affect the distribution (Figure 5D). In accord with the finding using the ATM inhibitor, the silencing of ATM did not affect the frequency, whereas the silencing of ATR reduced the frequency from 23.3% to 14.7% ($P < 0.01$) (Figure 5E). This observation was also confirmed in HT1080 cells with Rad51C dysfunction. The silencing of ATR reduced the frequency from 11.8% to 5.8% ($P < 0.01$) (Figure 5F). These results indicate that ATR but not ATM was involved in the generation of supernumerary centrosomes. Because treatment with ATR siRNA rescued centrosome aberrations related to Rad51C depletion, ATR is likely to promote the generation of supernumerary centrosomes in the damage response signaling pathway rather than in a pathway directly associated with Rad51C.

Chk1 is involved in promoting centrosome aberrations

Since Chk1 is activated by ATR in response to DNA damage, we examined the effect of Chk1 inhibition on centrosome aberrations by treatment with the Chk1 inhibitor UCN-01 at the concentration of 100 nM in the mutant cells. This treatment reduced the frequency of centrosome aberrations from 33.0% to 19.7% ($P < 0.01$) (Figure 6A). Although UCN-01 was originally shown to inhibit Chk1 rather than Chk2, a subsequent study using GST-Cdc25C (200–256) as a substrate showed that the drug inhibited the immunoprecipitated kinase activities of Chk1 and Chk2 from wild-type HCT116 cells after exposure to ionizing radiation (25). We examined inhibition of both kinases by the drug using GST-Cdc25C (200–256) as a substrate in the mutant cells. In accord with the previous result, UCN-01 inhibited both kinases (Figure 6B). To determine which kinase is involved in the generation of supernumerary centrosomes, we examined the effect of RNA interference of the kinases on the centrosome aberrations (Figure 6C). Treatment with Chk1 or Chk2 siRNA did not affect the cell-cycle distribution of the mutant cells (Figure 5D). Silencing of Chk1 by RNA interference reduced the frequency from 30.0% to 17.3%, whereas silencing of Chk2 did not affect the frequency (Figure 6D). These results indicate that the ATR-Chk1 pathway was involved in the generation of supernumerary centrosomes.

Rad51C dysfunction promotes centrosomal accumulation of Chk1

Chk1 was shown to localize to centrosomes in response to the DNA damage induced by ultraviolet irradiation or HU treatment (26). This observation suggested that accumulation of Chk1 at centrosomes contributes to its checkpoint functions. We examined centrosomal localization of Chk1 by double immunofluorescence of Chk1 and pericentrin in HCT116 cells (Figure 6E and F). In accord with the previous report, ultraviolet irradiation or hydroxyurea treatment promoted Chk1's centrosomal localization in HCT116 cells. The frequency of cells in which Chk1 localizes to centrosomes was 12.0% in wild-type

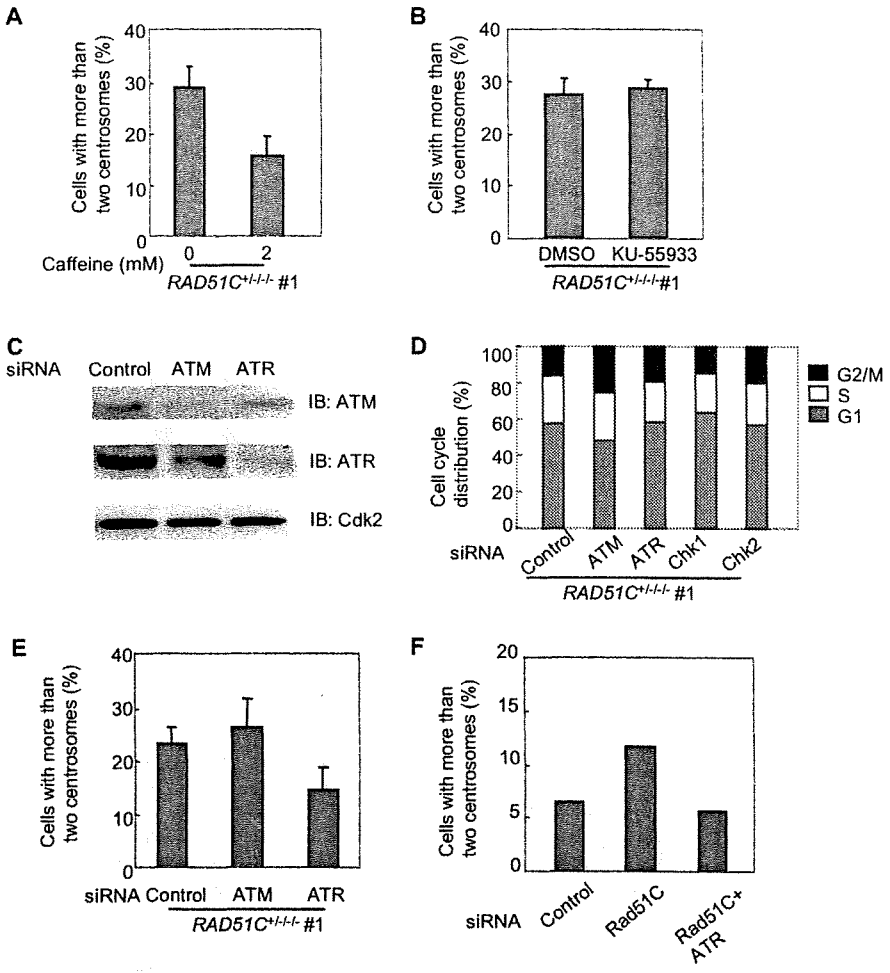

Figure 5. ATR-dependent centrosome aberrations. **(A)** Effect of caffeine treatment on centrosome aberrations in the Rad51C mutant cells. The cells were treated with 2 mM caffeine for 40 h. **(B)** Effect of an ATM inhibitor on centrosome aberrations in the Rad51C mutant cells. The cells were treated with either DMSO alone or 10 μM KU55933 dissolved in DMSO for 24 h. **(C)** Western blot analysis showing the expression of ATM and ATR in cells treated with siRNAs. **(D)** Cell-cycle distribution of the mutant cells treated with siRNAs. **(E)** Effect of silencing of ATM and ATR on centrosome aberrations in the Rad51C mutant cells. The frequencies of centrosome aberrations were examined in the cells treated with control, ATM or ATR siRNA. In (A), (B) and (E), a total of 100 cells were counted for each measurement. The results represent the means ± SEM of three independent experiments. **(F)** Effect of ATR silencing on centrosome aberrations in HT1080 cells treated with Rad51C siRNA. A total of 300 cells were counted.

cells, whereas it was 25.8% in the mutant cells ($P < 0.01$). We next examined focus formation of phosphorylated form of histone H2AX (γH2AX) in the nucleus by immunofluorescence of the protein. γH2AX is recruited to DSBs in response to DNA damage. γH2AX-positive cells were defined as cells harboring the discrete large-sized foci of the protein. The frequency of γH2AX-positive cells was 4.3% in wild-type cells, whereas it was increased to 55.7% in the mutant cells (Figure 6G). These observations indicate that Chk1 accumulates at centrosomes in response to unrepaired DNA damage caused by Rad51C dysfunction in the absence of exogenous insults. In addition, localization of Chk1 at centrosomes in response to DNA damage induced by ultraviolet irradiation or hydroxyurea treatment was promoted by Rad51C dysfunction. Together with our observation that the Rad51C mutant cells were hypersensitive to HU (Figure 2C), these results suggest that Rad51C dysfunction may lead to prolonged replication fork arrest.

Rad51C dysfunction leads to increased aneuploidy

Supernumerary centrosomes are assumed to play a role in the generation of aneuploidy by inducing aberrant chromosome segregation. The frequency of aneuploidy, characterized by one or three chromosomes, was investigated by FISH using two independent chromosome-specific centromere probes (Figure 7A). The frequencies

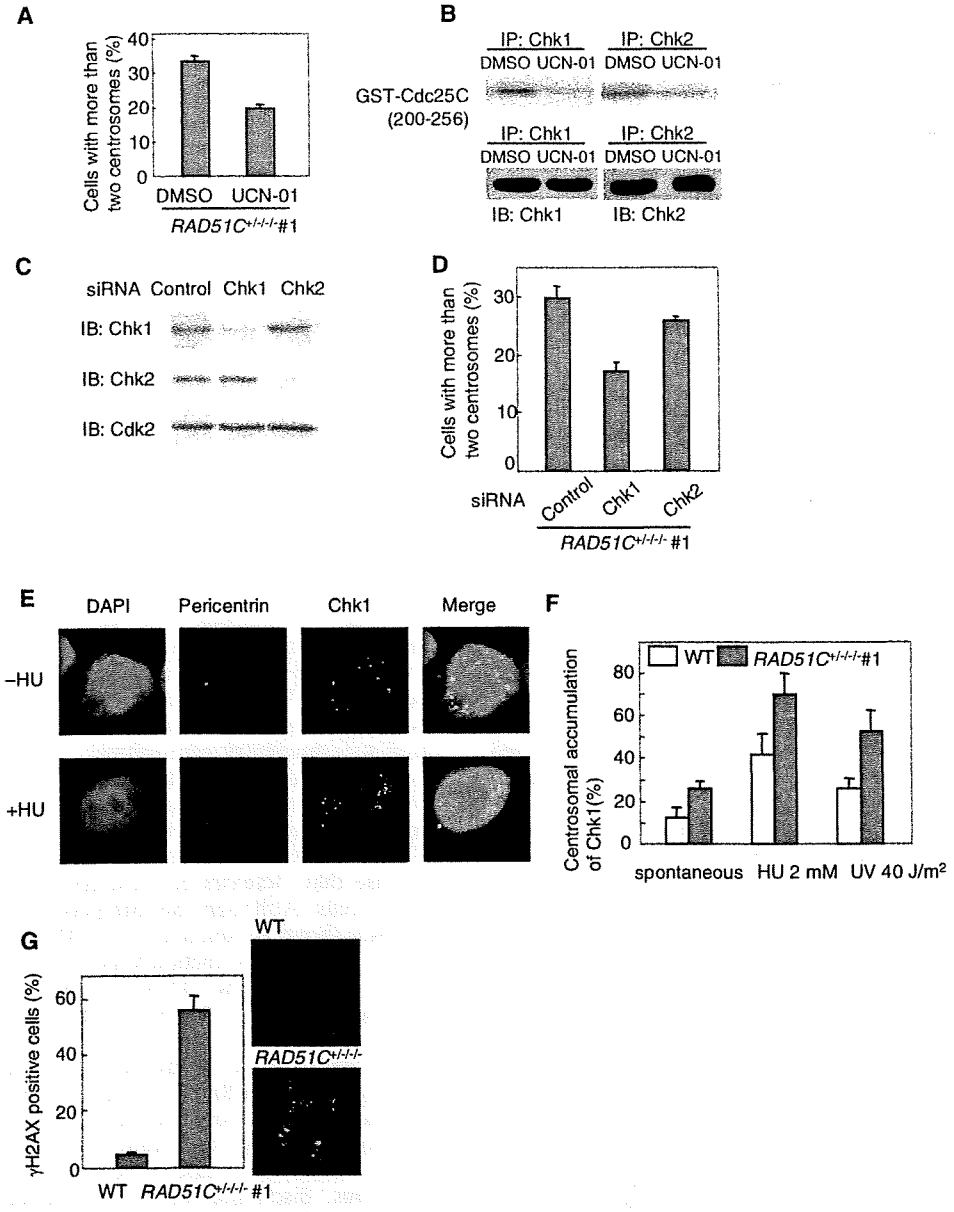

Figure 6. Chk1-dependent centrosome aberrations. **(A)** Effect of a Chk1 inhibitor on centrosome aberrations in the Rad51C mutant cells. The cells were treated with either DMSO alone or 100 nM UCN-01 dissolved in DMSO for 48 h. **(B)** Effect of UCN-01 on Chk1 and Chk2 kinase activities in the mutant cells. The cells were treated with 100 nM UCN-01 for 1 h. **(C)** Western blot analysis showing the expression of Chk1 and Chk2 in cells treated with siRNAs. **(D)** Effect of silencing of Chk1 and Chk2 on centrosome aberrations in the Rad51C mutant cells. The frequencies of centrosome aberrations were examined in the cells treated with control, Chk1 or Chk2 siRNA. **(E)** Damage-induced centrosomal accumulation of Chk1. HU treatment induces the accumulation of Chk1 at the centrosome. **(F)** Accumulation of Chk1 at the centrosome. **(G)** Focus formation of γH2AX in the nucleus. Immunofluorescence was carried out using the anti-γH2AX antibody. In (A), (D), (F) and (G), a total of 100 cells were counted for each measurement. The results represent the means ± SEM of three independent experiments.

of aneuploidy at chromosomes 7 and 17 were 3.3% and 3.4%, respectively, in wild-type cells, whereas they were increased to 7.4% and 7.6% in the Rad51C mutant cells ($P < 0.01$, Fisher's exact test) (Figure 7B). This indicates that Rad51C, like other Rad51 paralogs, maintains chromosome stability.

DISCUSSION

We have shown here that Rad51C dysfunction leads to increases in supernumerary centrosomes in an ATR-Chk1-dependent manner and to aneuploidy in human cells. This observation indicates that the DNA

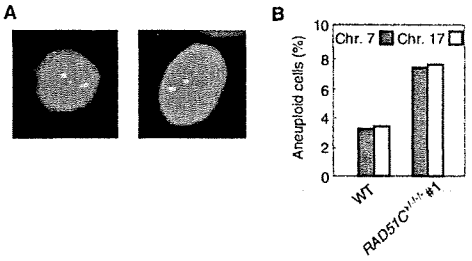

Figure 7. Increased aneuploidy. (**A**) FISH on Rad51C mutant cells using a probe for chromosome 7 (orange) and a probe for chromosome 17 (green). (**B**) Frequency of aneuploidy. For each chromosome-specific FISH, 500 cells were counted.

damage-response signal activated by Rad51C dysfunction causes chromosome instability by affecting centrosome integrity.

In contrast to previous studies using CL-V4B cells (11,12), the present study demonstrated that centrosome aberrations were induced by Rad51C dysfunction at both mitosis and interphase in two independent human cell lines. Since centrosome aberrations in interphase are likely to be generated at the S and G2 phases, such a difference may be explained by a mechanism that regulates centrosome integrity at these phases of the cell cycle. Given that the DNA damage response is involved in the maintenance of centrosome integrity, the absence of a protein involved in the signaling in response to unrepaired DNA damage may explain the lack of centrosome aberrations in interphase in CL-V4B cells.

A defect in the mismatch repair pathway has been shown to interfere with the DNA damage response (27). Since MLH1, a mismatch repair protein, is mutated in HCT116 cells, some phenotypes observed in the derivatives of this cell line are likely to be affected by a defect in mismatch repair. However, ATR-dependent centrosome aberrations in interphase were also observed in mismatch-proficient HT1080 cells, thus excluding this possibility.

The present results, together with those of previous studies (8–10,12), strengthen the role of Rad51 paralogs in the maintenance of centrosome integrity. However, it is unlikely that Rad51 paralogs directly regulate centrosome functions. There is no evidence to suggest that any member of the Rad51 paralog family localizes to the centrosome (7). We confirmed that Rad51C does not localize to the centrosome by exogenous expression of the *RAD51C* cDNA fused with the green fluorescent protein in Rad51C mutant cells (data not shown). Since Rad51C participates in the formation of two protein complexes consisting of five members of the Rad51 paralog family, these complexes are unlikely to localize to the centrosome.

Evidence that the DNA damage response plays a role in centrosome functions has been accumulating. ATM, ATR, ATRIP, Chk1 and Chk2 were shown to localize to the centrosome in HeLa cells (28). Supernumerary centrosomes in human lymphoblastoid cells exposed to ionizing radiation were cancelled by treatment with 2 mM caffeine or by the depletion of Chk1, suggesting that the ATM/ATR-Chk1 pathway may be involved in promoting centrosome amplification induced by DNA damage (16). The ATR-Chk1 pathway's role in regulating centrosome functions has been proposed from the identification of mutations in pericentrin, a centrosomal protein, in Seckel syndrome as well as in Majewski osteodysplastic primordial dwarfism type II (MOPD II) syndrome (29,30). These rare genetic disorders share dwarfism and microcephaly. Since ATR mutations are responsible for Seckel syndrome (31), the ATR-dependent DNA damage response signaling pathway might be associated with the pericentrin-dependent pathway. Although the exact role of ATR in centrosome functions remains to be elucidated, these results support the present finding that ATR is involved in increased supernumerary centrosomes. It is also noteworthy that caffeine treatment in Rad51C mutant cells did not reduce the frequency of centrosome aberrations to the wild-type levels, suggesting that an ATR-independent pathway may play a minor role in promoting centrosome aberrations in the mutant cells.

Defective homologous recombination causes prolonged replication fork arrest. Increased centrosome numbers that arise spontaneously in Rad51C mutant cells are likely to be attributable to prolonged arrest at replication forks or at the G2/M boundary. Furthermore, the present finding that ATR or Chk1 depletion reduced centrosome aberrations suggests that prolonged checkpoint arrest may cause supernumerary centrosomes. The previous finding that centrosome amplification induced by Rad51 deletion was caused during the prolonged G2 phase in an ATM-dependent manner supports this model (13). However, ATM is unlikely to be involved in the DNA damage response that increases centrosome numbers in Rad51C mutant cells. Although the interplay between ATM and ATR was shown to function in the DNA damage response (32,33), Rad51C dysfunction appears to activate the ATR-specific pathway. The DNA damage response signaling pathway activated by Rad51C dysfunction may be different from the pathway activated by depletion of Rad51. Rad51C may play a role in the DNA repair process that does not depend on Rad51. Rad51C or its associated proteins have been proposed to have a resolvase activity for Holliday junctions, suggesting that Rad51C may be involved in the late phase of homologous recombination (34). Thus, discrimination in the choice of the DNA damage response signal in their mutant cells may reflect functional differences between Rad51 and Rad51C in DSB repair through homologous recombination.

FUNDING

Japanese Society for Promoting Science (18310037 to K.M.); the Ministry of Education, Culture, Sports, Science and Technology (18012012 to K.M.); the Ministry of Health, Labor and Welfare of Japan (19140401 to K.M.); Hiroshima University 21st Century Center of Excellence Program (M.K. and T.Y.). Funding for open access charge: Japanese Society for Promoting Science.

Conflict of interest statement. None declared.

REFERENCES

1. West,S.C. (2003) Molecular views of recombination proteins and their control. *Nat. Rev. Mol. Cell Biol.*, **4**, 435–445.
2. Thacker,J. (2005) The RAD51 gene family, genetic instability and cancer. *Cancer Lett.*, **219**, 125–135.
3. Masson,J.-Y., Tarsounas,M.C., Stasiak,A.Z., Stasiak,A., Shah,R., McIlwraith,M.J., Benson,F.E. and West,S.C. (2001) Identification and purification of two distinct complexes containing the five RAD51 paralogs. *Genes Dev.*, **15**, 3296–3307.
4. Liu,N., Schild,D., Thelen,M.P. and Thompson,L.H. (2002) Involvement of Rad51C in two distinct protein complexes of Rad51 paralogs in human cells. *Nucleic Acids Res.*, **30**, 1009–1015.
5. Bettencourt-Dias,M. and Glover,D.M. (2007) Centrosome biogenesis and function: centrosomics brings new understanding. *Nat. Rev. Mol. Cell Biol.*, **8**, 451–463.
6. Nigg,E.A. (2006) Origins and consequences of centrosome aberrations in human cancers. *Int. J. Cancer*, **119**, 2717–2723.
7. Doxsey,S., Zimmerman,W. and Mikule,K. (2005) Centrosome control of the cell cycle. *Trends Cell Biol.*, **15**, 303–311.
8. Griffin,C.S., Simpson,P.J., Wilson,C.R. and Thacker,J. (2000) Mammalian recombination-repair genes XRCC2 and XRCC3 promote correct chromosome segregation. *Nat. Cell Biol.*, **2**, 757–761.
9. Smiraldo,P.G., Gruver,A.M., Osborn,J.C. and Pittman,D.L. (2005) Extensive chromosomal instability in Rad51d-deficient mouse cells. *Cancer Res.*, **65**, 2089–2096.
10. Date,O., Katsura,M., Ishida,M., Yoshihara,T., Kinomura,A., Sueda,T. and Miyagawa,K. (2006) Haploinsufficiency of RAD51B causes centrosome fragmentation and aneuploidy in human cells. *Cancer Res.*, **66**, 6018–6024.
11. Godthelp,B.C., Wiegant,W.W., van Duijn-Goedhart,A., Scharer,O.D., van Buul,P.P.W., Kanaar,R. and Zdzienicka,M.Z. (2002) Mammalian Rad51C contributes to DNA cross-link resistance, sister chromatid cohesion and genomic stability. *Nucleic Acids Res.*, **30**, 2172–2182.
12. Lindh,A.R., Schultz,N., Saleh-Gohari,N. and Helleday,T. (2007) RAD51C (RAD51L2) is involved in maintaining centrosome number in mitosis. *Cytogenet. Genome Res.*, **116**, 38–45.
13. Dodson,H., Bourke,E., Jeffers,L.J., Vagnarelli,P., Sonoda,E., Takeda,S., Earnshaw,W.C., Merdes,A. and Morrison,C. (2004) Centrosome amplification induced by DNA damage occurs during a prolonged G2 phase and involves ATM. *EMBO J.*, **23**, 3864–3873.
14. Daboussi,F., Thacker,J. and Lopez,B.S. (2005) Genetic interactions between RAD51 and its paralogues for centrosome fragmentation and ploidy control, independently of the sensitivity to genotoxic stresses. *Oncogene*, **24**, 3691–3696.
15. Pujana,M.A., Han,J.D., Starita,L.M., Stevens,K.N., Tewari,M., Ahn,J.S., Rennert,G., Moreno,V., Kirchhoff,T., Gold,B *et al.* (2007) Network modeling links breast cancer susceptibility and centrosome dysfunction. *Nat. Genet.*, **39**, 1338–1349.
16. Bourke,E., Dodson,H., Merdes,A., Cuffe,L., Zachos,G., Walker,M., Gillespie,D. and Morrison,C.G. (2007) DNA damage induces Chk1-dependent centrosome amplification. *EMBO Rep.*, **8**, 603–609.
17. Miyagawa,K., Tsuruga,T., Kinomura,A., Usui,K., Katsura,M., Tashiro,S., Mishima,H. and Tanaka,K. (2002) A role for RAD54B in homologous recombination in human cells. *EMBO J.*, **21**, 175–180.
18. Yoshihara,T., Ishida,M., Kinomura,A., Katsura,M., Tsuruga,T., Tashiro,S., Asahara,T. and Miaygawa,K. (2004) XRCC3 deficiency results in a defect in recombination and increased endoreduplication in human cells. *EMBO J.*, **23**, 670–680.
19. Yokoyama,H., Kurumizaka,H., Ikawa,S., Yokoyama,S. and Shibata,T. (2003) Holliday junction binding activity of the human Rad51B protein. *J. Biol. Chem.*, **278**, 2767–2772.
20. Hiyama,T., Katsura,M, Yoshihara,T., Ishida,M., Kinomura,A., Tonda,T., Asahara,T. and Miyagawa,K. (2006) Haploinsufficiency of the Mus81-Eme1 endonuclease activates the intra-S-phase and G_2/M checkpoints and promote rereplication in human cells. *Nucleic Acids Res.*, **34**, 880–892.
21. Bärlund,M., Monni,O., Kononen,J., Cornelison,R., Torhorst,J., Sauter,G., Kallioniemi,O-P. and Kallioniemi,A. (2000) Multiple genes at 17q23 undergo amplification and overexpression in breast cancer. *Cancer Res.*, **60**, 5340–5344.
22. Wu,G.-J., Sinclair,C.S., Paape,J., Ingle,J.N., Roche,P.C., James,C.D. and Couch,F.J. (2000) 17q23 amplifications in breast cancer involve the PAT1, RAD51C, PS6K, and SIGMA1B genes. *Cancer Res.*, **60**, 5371–5375.
23. Takata,M., Sasaki,M.S., Tachiiri,S., Fukushima,T., Sonoda,E., Schild,D., Thompson,L.H. and Takeda,S. (2001) Chromosome instability and defective recombinational repair in knockout mutants of the five Rad51 paralogs. *Mol. Cell Biol.*, **21**, 2858–2866.
24. Lio,Y.-C., Schild,D., Brenneman,M.A., Redpath,J.L. and Chen,D.J. (2004) Human Rad51C deficiency destabilizes XRCC3, impairs recombination, and radiosensitizes S/G2-phase cells. *J. Biol. Chem.*, **279**, 42313–42320.
25. Yu,Q., La Rose,J., Zhang,H., Takemura,H., Kohn,K.W. and Pommier,Y. (2002) UCN-01 inhibits p53 up-regulation and abrogates γ-radiation-induced G_2-M checkpoint independently of p53 by targeting both of the checkpoint kinases, Chk2 and Chk1. *Cancer Res.*, **62**, 5743–5748.
26. Löffler,H., Bochtler,T., Fritz,B., Tews,B., Ho,A.D., Lukas,J., Bartek,J. and Krämer,A. (2007) DNA damage-induced accumulation of centrosomal Chk1 contributes to its checkpoint function. *Cell Cycle*, **6**, 2541–2548.
27. Brown,K.D., Rathi,A., Kamath,R., Beardsley,D.I., Zhan,Q., Mannino,J.L. and Baskaran,R. (2003) The mismatch repair system is required for S-phase checkpoint activation. *Nat. Genet.*, **33**, 80–84.
28. Zhang,S., Hemmerich,P. and Grosse,F. (2007) Centrosomal localization of DNA damage checkpoint proteins. *J. Cell Biochem.*, **101**, 451–465.
29. Griffith,E., Walker,S., Martin,C.-A., Vagnarelli,P., Stiff,T., Vernay,B., Sanna,N.A., Saggar,A., Hamel,B., Earnshaw,W.C. *et al.* (2008) Mutations in pericentrin cause Seckel syndrome with defective ATR-dependent DNA damage signaling. *Nat. Genet.*, **40**, 232–236.
30. Rauch,A., Thiel,C.T., Schindler,D., Wick,U., Crow,Y.J., Ekici,A.B., van Essen,A.J., Goecke,T.O., Al-Gazali,L., Chrzanowska,K.H. *et al.* (2008) Mutations in the pericentrin (PCNT) gene cause primordial dwarfism. *Science*, **319**, 816–819.
31. O'Driscoll,M., Ruiz-Perez,V.L., Woods,C.G., Jeggo,P.A. and Goodship,J.A. (2003) A splicing mutation affecting expression of ataxia-telangiectasia and Rad3-related protein (ATR) results in Seckel syndrome. *Nat. Genet.*, **33**, 497–501.
32. Jazayeri,A., Falck,J., Lukas,C., Bartek,J., Smith,G.C.M., Lukas,J. and Jackson,S.P. (2006) ATM- and cell cycle-dependent regulation of ATR in response to DNA double-strand breaks. *Nat. Cell Biol.*, **8**, 37–45.
33. Stiff,T., Walker,S.A., Cerosaletti,K., Goodarzi,A.A., Petermann,E., Concannon,P., O'Driscoll,M. and Jeggo,P.A. (2006) ATR-dependent phosphorylation and activation of ATM in response to UV treatment or replication fork stalling. *EMBO J.*, **25**, 5775–5782.
34. Liu,Y., Masson,J.-Y., Shah,R., O'Regan,P. and West,S.C. (2004) RAD51C is required for Holliday junction processing in mammalian cells. *Science*, **303**, 243–246.

THE JOURNAL OF BIOLOGICAL CHEMISTRY VOL. 284, NO. 21, pp. 14326–14336, May 22, 2009

Recombination Activator Function of the Novel RAD51- and RAD51B-binding Protein, Human EVL*[S]

Received for publication, October 6, 2008, and in revised form, March 25, 2009 Published, JBC Papers in Press, March 26, 2009, DOI 10.1074/jbc.M807715200

Motoki Takaku[‡], Shinichi Machida[‡], Noriko Hosoya[§], Shugo Nakayama[‡], Yoshimasa Takizawa[‡], Isao Sakane[‡], Takehiko Shibata[¶], Kiyoshi Miyagawa[§], and Hitoshi Kurumizaka[‡1]

From the [‡]Laboratory of Structural Biology, Graduate School of Advanced Science and Engineering, and Consolidated Research Institute for Advanced Science and Medical Care, Waseda University, 2-2 Wakamatsu-cho, Shinjuku-ku, Tokyo 162-8480, the [§]Laboratory of Molecular Radiology, Center of Disease Biology and Integrative Medicine, Graduate School of Medicine, University of Tokyo, 7-3-1 Hongo, Bunkyo-ku, Tokyo 113-0033, and the [¶]RIKEN Advanced Science Institute, 2-1 Hirosawa, Wako-shi, Saitama 351-0198, Japan

The RAD51 protein is a central player in homologous recombinational repair. The RAD51B protein is one of five RAD51 paralogs that function in the homologous recombinational repair pathway in higher eukaryotes. In the present study, we found that the human EVL (Ena/Vasp-like) protein, which is suggested to be involved in actin-remodeling processes, unexpectedly binds to the RAD51 and RAD51B proteins and stimulates the RAD51-mediated homologous pairing and strand exchange. The EVL knockdown cells impaired RAD51 assembly onto damaged DNA after ionizing radiation or mitomycin C treatment. The EVL protein alone promotes single-stranded DNA annealing, and the recombination activities of the EVL protein are further enhanced by the RAD51B protein. The expression of the EVL protein is not ubiquitous, but it is significantly expressed in breast cancer-derived MCF7 cells. These results suggest that the EVL protein is a novel recombination factor that may be required for repairing specific DNA lesions, and that may cause tumor malignancy by its inappropriate expression.

Chromosomal DNA double strand breaks (DSBs)[2] are potential inducers of chromosomal aberrations and tumorigenesis, and they are accurately repaired by the homologous recombinational repair (HRR) pathway, without base substitutions, deletions, and insertions (1–3). In the HRR pathway (4, 5), single-stranded DNA (ssDNA) tails are produced at the DSB sites. The RAD51 protein, a eukaryotic homologue of the bacterial RecA protein, binds to the ssDNA tail and forms a helical nucleoprotein filament. The RAD51-ssDNA filament then binds to the intact double-stranded DNA (dsDNA) to form a three-component complex, containing ssDNA, dsDNA, and the RAD51 protein. In this three-component complex, the RAD51 protein promotes recombination reactions, such as homologous pairing and strand exchange (6–9).

The RAD51 protein requires auxiliary proteins to promote the homologous pairing and strand exchange reactions efficiently in cells (10–12). In humans, the RAD52, RAD54, and RAD54B proteins directly interact with the RAD51 protein (13–17) and stimulate the RAD51-mediated homologous pairing and/or strand exchange reactions *in vitro* (18–21). The human RAD51AP1 protein, which directly binds to the RAD51 protein (22), was also found to stimulate RAD51-mediated homologous pairing *in vitro* (23, 24). The BRCA2 protein contains ssDNA-binding, dsDNA-binding, and RAD51-binding motifs (25–33), and the *Ustilago maydis* BRCA2 ortholog, Brh2, reportedly stimulated RAD51-mediated strand exchange (34, 35). Most of these RAD51-interacting factors are known to be required for efficient RAD51 assembly onto DSB sites in cells treated with ionizing radiation (10–12).

The RAD51B (RAD51L1, Rec2) protein is a member of the RAD51 paralogs, which share about 20–30% amino acid sequence similarity with the RAD51 protein (36–38). *RAD51B*-deficient cells are hypersensitive to DSB-inducing agents, such as cisplatin, mitomycin C (MMC), and γ-rays, indicating that the RAD51B protein is involved in the HRR pathway (39–44). Genetic experiments revealed that *RAD51B*-deficient cells exhibited impaired RAD51 assembly onto DSB sites (39, 44), suggesting that the RAD51B protein functions in the early stage of the HRR pathway. Biochemical experiments also suggested that the RAD51B protein participates in the early to late stages of the HRR pathway (45–47).

In the present study, we found that the human EVL (Ena/Vasp-like) protein binds to the RAD51 and RAD51B proteins in a HeLa cell extract. The EVL protein is known to be involved in cytoplasmic actin remodeling (48) and is also overexpressed in breast cancer (49). Like the RAD51B knockdown cells, the EVL knockdown cells partially impaired RAD51 foci formation after DSB induction, suggesting that the EVL protein enhances RAD51 assembly onto DSB sites. The purified EVL protein preferentially bound to ssDNA and stimulated RAD51-mediated homologous pairing and strand exchange. The EVL protein also promoted the annealing of complementary strands. These recombination reactions that were stimulated or promoted by the EVL protein were further enhanced by the

* This work was supported in part by grants-in-aid from the Ministry of Education, Culture, Sports, Science, and Technology, Japan.
[S] The on-line version of this article (available at http://www.jbc.org) contains supplemental Figs. 1–3.
[1] To whom correspondence should be addressed. Tel.: 81-3-5369-7315; Fax: 81-3-5367-2820; E-mail: kurumizaka@waseda.jp.
[2] The abbreviations used are: DSB, double strand break; HRR, homologous recombinational repair; ssDNA, single-stranded DNA; dsDNA, double-stranded DNA; MMC, mitomycin C; NTA, nitrilotriacetic acid; HPLC, high performance liquid chromatography; SPR, surface plasmon resonance; DTT, dithiothreitol; AMPPNP, 5′-adenylyl-β,γ-imidodiphosphate; BSA, bovine serum albumin; siRNA, small interfering RNA.

RAD51B protein. These results strongly suggested that the EVL protein is a novel factor that activates RAD51-mediated recombination reactions, probably with the RAD51B protein. We anticipate that, in addition to its involvement in cytoplasmic actin dynamics, the EVL protein may be required in homologous recombination for repairing specific DNA lesions, and it may cause tumor malignancy by inappropriate recombination enhanced by EVL overexpression in certain types of tumor cells.

EXPERIMENTAL PROCEDURES

Purification of the Human EVL Protein—The human *EVL* gene was isolated from a human cDNA pool (purchased from Clontech) by polymerase chain reaction and was cloned in the pET-15b vector (Novagen). In this construct, the hexahistidine tag sequence was fused at the N-terminal end of the gene. The EVL protein was expressed in the *Escherichia coli* JM109(DE3) strain, which also carried an expression vector for the minor tRNAs (Codon(+)RIL; Stratagene). The cells producing the EVL protein were resuspended in buffer containing 20 mM potassium phosphate (pH 8.5), 700 mM NaCl, 5 mM 2-mercaptoethanol, 10 mM imidazole, and 10% glycerol and were disrupted by sonication. The cell debris was removed by centrifugation for 20 min at 30,000 × *g*, and the lysate was mixed gently by the batch method with Ni^{2+}-NTA-agarose beads (8 ml; Qiagen) at 4 °C for 1 h. The EVL-bound beads were washed with 80 ml of buffer containing 20 mM potassium phosphate (pH 8.5), 700 mM NaCl, 5 mM 2-mercaptoethanol, 30 mM imidazole, and 10% glycerol. The beads were then washed with 80 ml of buffer containing 20 mM potassium phosphate (pH 8.5), 700 mM NaCl, 5 mM 2-mercaptoethanol, 60 mM imidazole, and 10% glycerol and then were washed again with buffer containing 20 mM potassium phosphate (pH 8.5), 700 mM NaCl, 5 mM 2-mercaptoethanol, 30 mM imidazole, and 10% glycerol. The beads were then packed into an Econo-column (Bio-Rad) and were washed with 300 ml of buffer containing 20 mM potassium phosphate (pH 8.5), 100 mM NaCl, 5 mM 2-mercaptoethanol, 30 mM imidazole, and 10% glycerol. The His_6-tagged EVL protein was eluted with a 30-column volume linear gradient of 30–300 mM imidazole, in 20 mM potassium phosphate (pH 8.5), 100 mM NaCl, 5 mM 2-mercaptoethanol, and 10% glycerol. The fractions containing the His_6-tagged EVL protein were diluted with the same volume of buffer, containing 10 mM potassium phosphate (pH 8.5), 100 mM NaCl, 5 mM 2-mercaptoethanol, and 10% glycerol, and were mixed gently by the batch method with hydroxyapatite resin (10 ml; Bio-Rad) at 4 °C for 1 h. The resin was then washed with 80 ml of buffer, containing 20 mM potassium phosphate (pH 8.5), 100 mM NaCl, 5 mM 2-mercaptoethanol, and 10% glycerol, and was packed into an Econo-column (Bio-Rad). The resin was further washed with 300 ml of buffer, containing 20 mM potassium phosphate (pH 8.5), 225 mM NaCl, 5 mM 2-mercaptoethanol, and 10% glycerol, and then the His_6-tagged EVL protein was eluted with a 30-column volume linear gradient of 225–1000 mM NaCl and 10–300 mM potassium phosphate (pH 8.5). The His_6 tag was uncoupled from the EVL portion by a digestion with 5.5 units of thrombin protease (GE Healthcare) per mg of the His_6-tagged EVL protein, and then the protein was immediately dialyzed against buffer containing 20 mM potassium phosphate (pH 7.5), 200 mM NaCl, 5 mM 2-mercaptoethanol, and 10% glycerol at 4 °C. After uncoupling of the His_6 tag, the EVL protein was further purified by Superdex 200 gel filtration column (HiLoad 26/60 preparation grade; GE Healthcare) chromatography, followed by Mono S column chromatography. The peak fractions were diluted with the same volume of buffer, containing 20 mM potassium phosphate (pH 7.5), 5 mM 2-mercaptoethanol, and 10% glycerol, and were subjected to MonoS (GE Healthcare) column chromatography. The column was washed with 20 column volumes of buffer, containing 20 mM potassium phosphate (pH 7.5), 100 mM NaCl, 5 mM 2-mercaptoethanol, and 10% glycerol, and the EVL protein was eluted with a 12-column volume linear gradient of 100–600 mM NaCl. The purified EVL protein was dialyzed against buffer containing 20 mM HEPES-NaOH (pH 7.3), 100 mM NaCl, 5 mM 2-mercaptoethanol, and 30% glycerol and was stored at −80 °C. The concentration of the purified EVL protein was determined by the Bradford method, using bovine serum albumin (BSA) as the standard.

Purification of the Human RAD51, RAD51B, DMC1, and RPA Proteins—The human RAD51 protein (50), human RAD51B protein (47), human DMC1 protein (51), and human RPA protein (52) were purified by the methods described previously.

DNA Substrates—Single-stranded ϕX174 viral (+) strand DNA and double-stranded ϕX174 replicative form I DNA were purchased from New England Biolabs. The linear dsDNA was prepared from the ϕX174 replicative form I DNA by PstI digestion. In the D-loop formation assay, superhelical dsDNA (pB5Sarray DNA) was prepared by a method to prevent irreversible denaturation of the dsDNA substrate by alkaline treatment of the cells harboring the plasmid DNA. The cells were gently lysed using Sarkosyl, as described previously (15). The pB5Sarray DNA contained 11 repeats of a sea urchin 5 S rRNA gene (207-bp fragment) within the pBlueScript II SK(+) vector. For the ssDNA annealing assay, the following high performance liquid chromatography (HPLC)-purified oligonucleotides were purchased from Nihon Gene Research Laboratory: 5′-GTC CCA GGC CAT TAC AGA TCA ATC CTG AGC ATG TTT ACC AAG CGC ATT G-3′ and 5′-CAA TGC GCT TGG TAA ACA TGC TCA GGA TTG ATC TGT AAT GGC CTG GGA C-3′. For the ssDNA substrate used in the D-loop assay, the following HPLC-purified oligonucleotide was purchased: 50-mer, 5′-GGA ATT CGG TAT TCC CAG GCG GTC TCC CAT CCA AGT ACT AAC CGA GCC CT-3′. The DNA sequences used in the strand exchange assay with the oligonucleotides are as follows: 63-mer, 5′-TCC TTT TGA TAA GAG GTC ATT TTT GCG GAT GGC TTA GAG CTT AAT TGC TGA ATC TGG TGC TGT-3′; 32-mer top strand, 5′-CCA TCC GCA AAA ATG ACC TCT TAT CAA AAG GA-3′; 32-mer bottom strand, 5′-TCC TTT TGA TAA GAG GTC ATT TTT GCG GAT GG-3′. The 5′-ends of the oligonucleotide (32-mer bottom strand) were labeled with T4 polynucleotide kinase (New England Biolabs) in the presence of [γ-^{32}P]ATP at 37 °C for 30 min. All DNA concentrations are expressed in moles of nucleotides.

Pulldown Assays with EVL-conjugated Beads—The EVL protein was covalently conjugated to Affi-Gel 10 beads (100 μl;

Bio-Rad), according to the manufacturer's instructions. To block the remaining active ester sites, ethanolamine (pH 8.0) was added to a final concentration of 100 mM, and the resin was incubated at 4 °C overnight. The unbound proteins were removed by washing the Affi-Gel 10-EVL beads three times with 500 μl of binding buffer, which contained 20 mM HEPES-NaOH (pH 7.3), 100 mM NaCl, 5 mM 2-mercaptoethanol, 30% glycerol, and 0.05% Triton X-100. After washing the resin, the Affi-Gel 10-protein matrices were adjusted to 50% slurries and were stored at 4 °C.

For the RAD51B-binding and RAD51-binding assays, the EVL beads were incubated with a HeLa whole cell extract (2 mg of protein), and the beads were washed three times with 200 μl of washing buffer, containing 50 mM potassium phosphate (pH 7.5), 100 mM NaCl, 5 mM EDTA, 0.5% Nonidet P-40, and protease inhibitor mixture (Nacalai Tesque). The proteins that copelleted with the EVL beads were separated into two portions for the RAD51 and RAD51B analyses and were fractionated by 12% SDS-PAGE. The RAD51 and RAD51B proteins were detected with the RAD51-specific and RAD51B-specific rabbit polyclonal antibodies, respectively.

Pulldown Assays with the Ni^{2+}-NTA-Agarose Beads—The His_6-tagged EVL protein (0.45 μM) was prepared and was mixed with the RAD51 or RAD51B protein (2 μM) in 20 mM HEPES buffer (pH 7.3), containing 95 mM NaCl, 0.1 mM EDTA, 0.045% Triton X-100, 1.8 mM ammonium sulfate, 2 mM 2-mercaptoethanol, 4.5 mM imidazole, and 29% glycerol. After a 30-min incubation at room temperature, 1.5 μl of the Ni^{2+}-NTA-agarose beads were added to the reaction mixture, and the RAD51 or RAD51B protein bound to the His_6-tagged EVL protein was captured by the beads. The beads were washed two times with 100 μl of washing buffer, containing 20 mM HEPES-NaOH (pH 7.3), 90 mM NaCl, 0.1 mM EDTA, 0.05% Triton X-100, 2 mM ammonium sulfate, 2 mM 2-mercaptoethanol, 5 mM imidazole, and 30% glycerol. The proteins that copelleted with the Ni^{2+}-NTA beads were eluted with a buffer, containing 14 mM HEPES-NaOH (pH 7.3), 100 mM NaCl, 3.5 mM 2-mercaptoethanol, 300 mM imidazole, and 21% glycerol. The eluted fractions were analyzed by 12% SDS-PAGE with Coomassie Brilliant Blue staining.

Surface Plasmon Resonance Analysis—The surface plasmon resonance (SPR) signals were measured with a Biacore J instrument (GE Healthcare). Flow cells were maintained at 25 °C during the measurement, and the instrument was operated at the mid-flow rate (~30 μl/min). The EVL protein was conjugated to the activated surface of CM5 sensor chips (GE Healthcare), using the standard amine coupling conditions recommended by the manufacturer. The level of the conjugated EVL protein was 3,860 resonance units. Reference SPR signals of the flow cell containing a sensor chip without the EVL protein were subtracted from those of the SPR signals of the flow cell containing the EVL-conjugated sensor chip. The running buffer was 20 mM HEPES-NaOH (pH 7.3), 150 mM NaCl, 2 mM ammonium sulfate, 5% glycerol, and 0.05% Triton X-100. Before each binding assay, the sensor chip was regenerated by a 1-min wash with 10 mM NaOH and two 1-min washes with 20 mM citrate buffer (pH 2.65), followed by a 25-min wash with the running buffer. For each binding assay, 1 μM analyte solution (*i.e.* the RAD51 protein, the RAD51B protein, the DMC1 protein, or the BSA solution) was injected for 5 min.

Assays for DNA Binding—The φX174 circular ssDNA (20 μM) or the linearized φX174 dsDNA (20 μM) was mixed with the EVL protein in 10 μl of a standard reaction solution, containing 36 mM HEPES-NaOH buffer (pH 7.5) with 1 mM dithiothreitol, 4 mM 2-mercaptoethanol, 80 mM NaCl, 1 mM $MgCl_2$, 24% glycerol, and 0.1 mg/ml BSA. The reaction mixtures were incubated at 37 °C for 15 min and were then analyzed by 0.8% agarose gel electrophoresis in 1× TAE buffer (40 mM Tris acetate and 1 mM EDTA) at 3.3 V/cm for 2 h. The bands were visualized by ethidium bromide staining.

The D-loop Formation Assay—The indicated amount of the EVL protein was incubated in the presence or absence of the RAD51 protein (0.1 μM) at 37 °C for 5 min in the reaction buffer, containing 26 mM HEPES-NaOH (pH 7.5), 40 mM NaCl, 0.02 mM EDTA, 0.9 mM 2-mercaptoethanol, 5% glycerol, 1 mM $MgCl_2$, 1 mM DTT, 2 mM AMPPNP, and 0.1 mg/ml BSA. After this incubation, the ^{32}P-labeled 50-mer oligonucleotide (1 μM) was added, and the samples were further incubated at 37 °C for 5 min. The reactions were then initiated by the addition of the pB5Sarray superhelical dsDNA (60 μM) along with 9 mM $MgCl_2$ and were continued at 37 °C for 30 min. The reactions were stopped by the addition of 0.2% SDS and 1.5 mg/ml proteinase K and were further incubated at 37 °C for 15 min. After adding 6-fold loading dye, the deproteinized reaction products were separated by 1% agarose gel electrophoresis in 1× TAE buffer at 3.3 V/cm for 2.5 h. The gels were dried, exposed to an imaging plate, and visualized using an FLA-7000 imaging analyzer (Fujifilm).

Assays for Homologous Pairing with Oligonucleotides—For the homologous pairing assay with oligonucleotides, the RAD51 protein and the indicated amounts of the EVL protein were incubated with a 63-mer ssDNA (15 μM) in 10 μl of standard reaction buffer, containing 28 mM HEPES-NaOH (pH 7.5), 50 mM NaCl, 1 mM ATP, 1 mM DTT, 0.1 mg/ml BSA, 1 mM $MgCl_2$, 1 mM $CaCl_2$, 0.02 mM EDTA, 1.4 mM 2-mercaptoethanol, 20 mM creatine phosphate, 75 μg/ml creatine kinase, and 8% glycerol at 37 °C for 10 min. The strand exchange reaction was initiated by the addition of the 32-mer dsDNA (1.5 μM), which shared sequence homology with the 63-mer ssDNA. After a 30-min incubation at 37 °C, the reaction was stopped by the addition of 0.2% SDS and 1.5 mg/ml proteinase K. The reaction mixtures were further incubated for 10 min at 37 °C. After 6-fold loading dye was added, the reaction mixtures were subjected to 15% polyacrylamide gel electrophoresis in 0.5× TBE buffer (45 mM Tris, 45 mM boric acid, and 1 mM EDTA) at 10 V/cm for 5 h. The gels were dried, exposed to an imaging plate, and visualized using an FLA-7000 imaging analyzer.

Assay for Strand Exchange—The RAD51 protein (1 μM) and RPA (1 μM) were incubated with the indicated amounts of the EVL protein and/or the RAD51B protein at 30 °C for 10 min, in 8 μl of reaction buffer, containing 28 mM HEPES-NaOH (pH 7.5), 2.5 mM Tris-HCl (pH 7.5), 49 mM NaCl, 5 mM KCl, 0.03 mM EDTA, 1.1 mM 2-mercaptoethanol, 9% glycerol, 0.2 mM ammonium sulfate, 0.005% Triton X-100, 1 mM $MgCl_2$, 1 mM $CaCl_2$, 1.1 mM DTT, 1 mM ATP, 0.1 mg/ml BSA, 20 mM creatine phosphate, and 75 μg/ml creatine kinase. After this incubation,

ϕX174 circular ssDNA (20 μM) was added, and the samples were further incubated at 30 °C for 10 min. The reactions were then initiated by the addition of ϕX174 linear dsDNA (20 μM) and were continued at 30 °C for 60 min. The reactions were stopped by the addition of 0.2% SDS and 1.5 mg/ml proteinase K (Roche Applied Science) and were further incubated for 20 min. After adding 6-fold loading dye, the deproteinized reaction products were separated by 1% agarose gel electrophoresis in 1 × TAE buffer at 3.3 V/cm for 4 h. The products were visualized by SYBR Gold (Invitrogen) staining.

ssDNA Annealing Assay—The ssDNA oligonucleotide 49-mer (0.2 μM) was incubated with the indicated amounts of the EVL protein at 30 °C for 5 min in 9 μl of reaction buffer, containing 28 mM HEPES-NaOH (pH 7.5), 50 mM NaCl, 2 mM 2-mercaptoethanol, 12% glycerol, 0.1 mM $MgCl_2$, 1 mM DTT, and 0.1 mg/ml BSA. For the experiment with the RAD51B protein, the EVL protein was preincubated with the indicated amounts of the RAD51B protein at 30 °C for 10 min, in 8 μl of reaction buffer, containing 28 mM HEPES-NaOH (pH 7.5), 38 mM NaCl, 1.4 mM 2-mercaptoethanol, 12% glycerol, 0.4 mM ammonium sulfate, 0.01% Triton X-100, 1 mM $MgCl_2$, 1 mM DTT, 1 mM ATP, and 0.1 mg/ml BSA, before the addition of the ssDNA oligonucleotide. The reactions were initiated by the addition of 0.2 μM antisense ^{32}P-labeled 49-mer oligonucleotide. At the times indicated, the reactions were quenched with an excess of the unlabeled 49-mer oligonucleotide. The DNA substrates and products were deproteinized by 0.2% SDS and 1.5 mg/ml proteinase K at 30 °C for 10 min. The products were fractionated by 10% PAGE in 0.5× TBE. The gels were dried, exposed to an imaging plate, and visualized using an FLA-7000 imaging analyzer.

EVL and RAD51B Knockdown Experiments—Rabbit polyclonal antibodies for the EVL and RAD51B proteins were obtained with the purified recombinant EVL and RAD51B proteins as antigens. The RAD51 antibody was purchased from Calbiochem (anti-RAD51 Ab-1 rabbit polyclonal antibody), and the Cdk2 antibody was purchased from Santa Cruz Biotechnology (Anti-Cdk2 M2 rabbit polyclonal antibody). The siRNA duplexes (Stealth™ RNAi) were designed by the BLOCK-iT™ RNAi Designer (Invitrogen) and were purchased from Invitrogen. The siRNA sequences of EVL and RAD51B are as follows: 5′-CCAGUAAGAAAUGGGUACCAAUCAA-3′ (for EVL) and 5′-GAGGUGUCCAUGAACUUCUAU-GUAU-3′ (for RAD51B). The sequence of the control siRNA is 5′-CCAAGAAGUAAAUGGAACCUUGCAA-3′, in which the EVL siRNA sequence was shuffled. The cells were seeded in a 6-well plate. A 15-μl aliquot of siRNA (20 μM) was diluted with 185 μl of serum-free Dulbecco's modified Eagle's medium. In a separate tube, 2 μl of Dharma*FECT* 4 Transfection Reagent (Dharmacon) were diluted with 198 μl of serum-free Dulbecco's modified Eagle's medium, and the mixture was incubated at room temperature for 5 min. The diluted Dharma*FECT* 4 was combined with the diluted siRNA duplex, and the mixture was incubated at room temperature for 20 min. A 2-ml aliquot of Dulbecco's modified Eagle's medium was then added to the Dharma*FECT* 4-siRNA complex. This mixture was applied to the cells, which were then incubated at 37 °C for 48 h.

Western Blotting—The cells were harvested and were resuspended in lysis buffer, containing 50 mM Tris-HCl (pH 7.5), 100 mM NaCl, 5 mM EDTA, 0.5% Nonidet P-40, 1.7 μg/ml aprotinin, 50 nM cantharidin, 1 mM phenylmethylsulfonyl fluoride, and 10 nM microcystine. After a 30-min incubation on ice, the cell lysates were sonicated and were centrifuged at 20,000 × *g* for 5 min at 4 °C. The lysates (30 μg of protein/lane) were separated by 12% SDS-PAGE, and the proteins were transferred to a nitrocellulose membrane. The membrane was probed with anti-EVL rabbit polyclonal antibody, anti-RAD51B rabbit polyclonal antibody, or anti-Cdk2 rabbit polyclonal antibody and was developed using a horseradish peroxidase-conjugated anti-rabbit IgG antibody and the ECL Western blotting detection reagent (GE Healthcare).

Immunostaining—MCF7 cells were grown on glass coverslips and were either nontreated or irradiated with 8 or 20 grays, using the ^{137}Cs source in the Facilities for Biological Research, Department of Nuclear Engineering and Management, Graduate School of Engineering, University of Tokyo. At 2 h after irradiation, the cells were fixed in 4% paraformaldehyde for 10 min, washed with PBS, and permeabilized with 0.5% Triton X-100 and 0.1% SDS in PBS for 5 min. The coverslips were incubated for 1 h at 37 °C with an anti-RAD51 antibody diluted with blocking buffer (1% BSA in PBS) and were then washed again. The RAD51 foci were visualized by an incubation with a fluorescein isothiocyanate-conjugated secondary antibody diluted in blocking buffer for 30 min at 37 °C. The nuclei of the cells were stained with 4′,6′-diamidino-2-phenylindole.

For MMC treatment, the cells were incubated in medium containing 0.8 μg/ml MMC (KYOWA) for 1 h at 37 °C. The cells were then washed with PBS, incubated for 24 h at 37 °C, and immunostained as described above.

Sensitivity to MMC—MCF7 cells were treated with MMC in suspension for 1 h and were washed three times with PBS. The cells were then plated at a density of 2 × 10^3 cells/60-mm dish. After 12 days of culture, colonies were counted.

RESULTS

The EVL Protein Is Involved in RAD51 Assembly—To identify novel HRR factors, we screened a human cDNA library by the two-hybrid method, with the human RAD51 protein and/or the RAD51 paralogs as bait. We obtained 73 positive clones as putative RAD51B-interacting proteins and found that 30 clones among them contained *EVL* gene fragments. Six clones encoding the RAD51C protein, which is a known RAD51B-interacting protein, were also found among these positive clones, suggesting that the screening was properly performed.

Since RAD51B is known to be required for the RAD51 assembly onto DSB sites after exposure to ionizing radiation, we then tested whether the EVL protein functions in RAD51 assembly *in vivo*. To do so, we performed RNA interference experiments. A treatment with a short interfering RNA (siRNA) designed to target the EVL mRNA caused about a 90% reduction in the EVL level in MCF7 cells, as compared with the cells treated with a control siRNA (Fig. 1*A*). The siRNA designed to target the RAD51B mRNA caused about an 80% reduction in the RAD51B level, without influencing the EVL level (Fig. 1*A*).